Formation of the low-latitude boundary layer and cusp under the northward IMF: Simultaneous observations by Cluster and Double Star

Y. V. Bogdanova,[1,2] C. J. Owen,[1] M. W. Dunlop,[3] J. A. Wild,[4] J. A. Davies,[3] A. D. Lahiff,[1] M. G. G. T. Taylor,[5] A. N. Fazakerley,[1] I. Dandouras,[6] C. M. Carr,[7] E. A. Lucek,[7] and H. Rème[6]

Received 27 August 2007; revised 7 December 2007; accepted 5 March 2008; published 12 June 2008.

[1] On 28 February 2004 the configuration of the Cluster and Double Star TC1 satellites facilitated a simultaneous study of plasma properties inside the low-latitude boundary layer (LLBL) near the subsolar magnetopause and inside the midaltitude cusp during an interval with strong northward IMF. TC1, crossing the dayside magnetopause, observed a complex structure of boundary layers. We suggest that one part of the LLBL, characterized by high fluxes of magnetosheath-like electrons, is formed due to reconnection processes. We can identify three different plasma populations inside this region: on open field lines outside the magnetopause which are reconnected in the northern hemisphere lobe sector; on open field lines inside the magnetosphere which are reconnected in the northern hemisphere lobe sector and sink inside the magnetosphere; and on reclosed field lines, which undergo a second reconnection in the southern hemisphere lobe sector. Another part of the LLBL, characterized by equal fluxes of magnetosheath-like and plasma sheet populations, is formed by diffusion processes as strong pitch angle diffusion and formation of a loss cone are observed inside this region. Cluster, moving from the polar cap toward the dayside magnetosphere via the cusp region, crossed many different sublayers with different plasma properties. Comparison of plasma populations inside the different subregions of the LLBL and cusp shows that the complex LLBL observed at the dayside magnetopause maps into the midaltitude cleft/cusp region and that observed sublayers inside the cusp can be explained by reconnection in the lobe sector of one or both hemispheres and by diffusion processes.

Citation: Bogdanova, Y. V., et al. (2008), Formation of the low-latitude boundary layer and cusp under the northward IMF: Simultaneous observations by Cluster and Double Star, *J. Geophys. Res.*, *113*, A07S07, doi:10.1029/2007JA012762.

1. Introduction

[2] The low-latitude boundary layer (LLBL) is often observed during magnetopause crossings by satellites. The LLBL contains a mixture of magnetosheath and magnetospheric plasma populations and it is adjacent to the magnetopause inside the magnetosphere [e.g., *Haerendel et al.*, 1978; *Eastman and Hones*, 1979; *Paschmann*, 1979; *Keyser et al.*, 2005]. The thickness of this layer is variable, and it was shown that this boundary layer becomes thicker under northward interplanetary magnetic field (IMF) conditions [*Eastman and Hones*, 1979]. A statistical study showed that the boundary layer was observed in 90% of magnetopause crossings [*Eastman et al.*, 1996]. Outside the magnetopause, the magnetosheath boundary layer (MSBL) is also often detected [e.g., *Fuselier et al.*, 1997]. This boundary layer is populated by the mixture of pristine magnetosheath plasma, leaking magnetospheric plasma and heated magnetosheath plasma which was heated at the magnetopause current layer and mirrored from low altitudes [e.g., *Onsager et al.*, 2001].

[3] The LLBL plays an important role in the coupling between the solar wind and the magnetosphere. Across this boundary layer the energy and momentum from the solar wind transfer into the magnetospheric system. The LLBL has been extensively studied during last few decades (see AGU monograph *Low-Latitude Boundary Layer*, published

[1]Mullard Space Science Laboratory, University College London, Dorking, UK.
[2]Now at Department of Physics, La Trobe University, Melbourne, Victoria, Australia.
[3]Space Science and Technology Department, Rutherford Appleton Laboratory, Didcot, UK.
[4]Department of Communication Systems, Lancaster University, Lancaster, UK.
[5]Research and Scientific Support Department, European Space Agency, Noordwijk, Netherlands.
[6]Centre d'Etude Spatiale des Rayonnements, Centre National de la Recherche Scientifique, Toulouse, France.
[7]Space and Atmospheric Physics, Blackett Laboratory, Imperial College London, London, UK.

0148-0227/08/2007JA012762$09.00

in 2003); however, a number of important questions remain unanswered.

[4] First, the LLBL often exhibits complicated substructure. For example, *Song et al.* [1990], based on ISEE-1 data, showed that the LLBL consists of two sublayers. The first sublayer, called the outer boundary layer (OBL), is dominated by magnetosheath particles and the second sublayer, called the inner boundary layer (IBL), is dominated by the magnetospheric population. Inside the OBL the plasma density and temperature are almost stable, while across the IBL the plasma temperature strongly increases. In their observations, plasma inside the different layers is homogeneous and sharp boundaries exist between the two layers, suggesting that there is a little diffusion present. In an extended study, *Song et al.* [1993] showed that the structure of the boundary layer can be even more complicated and that for some examples, a middle boundary layer is present and that slight heating may occur in the boundary layers. In the case of two layers, the ion velocity distribution consists of a simple mixture of two populations whose ratio is systematically changing.

[5] Similar observations of the substructure of the LLBL were presented by *Le et al.* [1996]. They demonstrated that inside the OBL the heated magnetosheath plasma is observed with little or no magnetospheric population and inside the IBL a mixture of magnetosheath and magnetospheric plasma is observed. Their study was based only on the analysis of ion data. However, signatures in the ion and electron populations inside the outer and inner boundary layers may be different. *Vaisberg et al.* [2001] observations of the weakly structured LLBL during northward IMF are in agreement with the observations of *Song et al.* [1990, 1993] and *Le et al.* [1996]. They demonstrated that the LLBL may consist of two regions, separated by a thin boundary, and that the number density profile is monotonic across the sharp boundaries. *Vaisberg et al.* [2001] also showed that the IBL is a mixture of both populations and that the trapped magnetospheric population is always observed in the inner LLBL and may also be observed in the outer LLBL. *Bauer et al.* [2001] performed an extended statistical study of the outer and inner boundary layers using data from the AMPTE/IRM satellite. They showed that the plasma in the OBL is dominated by solar wind particles and that the partial densities of the solar wind and magnetospheric particles are comparable inside the IBL. They also showed that ''warm,'' counterstreaming electrons that originate primarily from the magnetosheath and have a field-aligned temperature that is higher than the electron temperature in the magnetosheath by a factor of 1–5 are characteristic feature of the IBL. These ''warm'' bidirectional electrons overlap with the hot electron populations inside the IBL. In this statistical study, inside the OBL the density plateau is often observed and the plasma density exhibits step-like profiles inside the outer and inner boundary layers. One of the important findings from this study is that the step-like substructure of the LLBL is observed during any orientation of the IMF.

[6] The mechanism for the formation of the boundary layer is also somewhat controversial. There are a few mechanisms which can contribute to the plasma transfer across the boundary layer. First, the plasma diffusion may occur across the magnetopause. Plasma interaction with lower hybrid waves near the magnetopause may lead to localized field structure and enhanced diffusion rates through turbulence [e.g., *Shapiro et al.*, 1994]. However, in general the diffusion coefficients are not high enough to explain the formation of the LLBL [*Treumann et al.*, 1995]. Recently, *Bauer et al.* [2001] estimated the diffusion caused by lower hybrid drift instability, gyroresonant pitch angle scattering and kinetic Alfven wave turbulence and suggested that cross-field diffusion cannot transport solar wind plasma into the outer and inner boundary layers at a rate that would account for their thicknesses. It was pointed out that the diffusion process cannot explain the OBL formation where the density plateau is observed, as it predicts gradient regions only. Other mechanisms which can be responsible for the formation of the boundary layer are curvature drift, gradient B drift, and polarization drift, which must always contribute to the formation of the boundary layer to some degree [e.g., *Bauer et al.*, 2001]. However, it was shown that the estimated drift entry can only give a small contribution to the LLBL formation [*Treumann and Baumjohann*, 1988].

[7] The other candidate mechanism for the LLBL formation involves large-scale waves at the magnetopause: plasma may be transferred across the flank boundary via the Kelvin-Helmholtz instability [*Ogilvie and Fitzenreiter*, 1989; *Fujimoto and Teresawa*, 1995]. Mixing of the plasma from different sources, magnetosheath and magnetosphere, near the flanks is observed in the presence of the Kelvin-Helmholtz waves [*Hasegawa et al.*, 2004] and it has been suggested that localized reconnection can happen inside the plasma vortices [*Nykyri et al.*, 2006]. However, the KHI occurs at the flank of the magnetosphere and thus this process cannot explain the observations of the LLBL near the subsolar magnetopause.

[8] The last formation mechanism involves reconnection between terrestrial and magnetosheath field lines. During southward IMF reconnection occurs at the dayside magnetopause [*Dungey*, 1961] and the LLBL forms due to the time-of-flight effect of the energetic electrons, energetic ions, and the bulk plasma population accelerated at the magnetopause [*Gosling et al.*, 1990]. During northward IMF, reconnection is more likely to occur poleward of the cusp region, in the lobe sector [e.g., *Dungey*, 1963; *Crooker*, 1979]. All physically possible reconnection geometries during northward IMF were described by *Cowley* [1973, 1983] and include single lobe reconnection, dual lobe reconnection, and sequential merging. During single lobe reconnection, the IMF field lines reconnect with open lobe field lines in one hemisphere [e.g., *Milan et al.*, 2000; *Frey et al.*, 2002]. During dual lobe reconnection, which may occur under strong northward IMF, open field lines from both lobes reconnect with part of the magnetosheath field lines, thus creating newly reclosed field lines with captured magnetosheath plasma on them [*Song and Russell*, 1992; *Song et al.*, 2002]. These newly reclosed field lines will sink into the magnetosphere and due to the interchange instability will move antisunward around the flanks, thus forming a thick LLBL and cold dense plasma sheet, often observed during northward IMF [e.g., *Øieroset et al.*, 2005]. The sequential merging process is similar to dual lobe reconnection; however, reconnection processes at both hemispheres do not occur simultaneously. Recently,

Watanabe et al. [2006] introduced a new mode of sequential and internal reconnection, suggesting that during intervals with northward IMF and significant dipole tilt reconnection occurs not only between a summer lobe and a winter lobe field lines but also between a summer lobe field line and a closed field line.

[9] The Song and Russell mechanism [e.g., *Song and Russell*, 1992] can explain observations of magnetosheath-like plasma inside the LLBL. This mechanism was modified by *Le et al.* [1996] in order to explain observations of both the inner and outer layers of the LLBL. They suggested that lobe reconnection in both hemispheres does not happen simultaneously. In their model, the outer boundary layer appears to be formed by reconnection between magnetosheath and lobe field lines poleward of one cusp. Thus, it is on open field lines. The inner boundary layer is identified to be on closed field lines that have become closed by reconnection of the open end of the flux tube poleward of the other cusp. The mixture of the magnetosheath and magnetospheric populations inside the inner boundary layer was explained by the drift of hot magnetospheric plasma on these closed field lines, even if the hot plasma was completely absent when the field lines were open [*Mitchell et al.*, 1987].

[10] In observations reported by *Le et al.* [1996] there is a substantial difference in the plasma density of the outer and inner boundary layers. In one of the presented events, the outer boundary layer (on field lines reconnected once) has plasma density $\sim$ 20 cm^{-3}, while in the inner boundary layer (on field lines reconnected twice) the plasma density is $\sim$3–4 cm^{-3}. Such a big difference in plasma density is in agreement with observations by *Song et al.* [1990, 1993]. However, *Onsager et al.* [2001] presented Polar observations of the high-latitude cusp region and of the MSBL during northward IMF, which they interpreted as evidence for the satellite crossing once- or twice-reconnected field lines. In their observations, the differences in the plasma density on once- and twice-reconnected field lines are insignificant. Similar observations with almost equal plasma densities on field lines reconnected once or twice inside the high-latitude cusp region were presented in the study by *Bogdanova et al.* [2005]. Thus, it is still unclear what plasma density variations should be expected inside the outer and inner boundary layers.

[11] There are a few complications in the study of the LLBL using satellite data. Inside the magnetosheath boundary layer, the directionality of heated electrons is a good indicator of the field topology [*Fuselier et al.*, 1995, 1997; *Onsager et al.*, 2001; *Onsager and Scudder*, 2002] as it clearly shows if reconnection occurs in the lobe sector of one or both hemispheres [*Onsager et al.*, 2001; *Lavraud et al.*, 2005; *Lavraud et al.*, 2006]. However, determining the topology of the magnetic field lines inside the LLBL is more difficult as it is hard to distinguish the magnetic field topology based on plasma observations [e.g., *Phan et al.*, 1997]. Inside the magnetosphere, trapped magnetospheric electron distributions may indicate a closed topology [e.g., *Mitchell et al.*, 1987]. Other evidence of the closed topology is the counterstreaming electrons of low ($\sim$10 eV) and medium energy (50–400 eV) [*Ogilvie et al.*, 1984; *Hall et al.*, 1991]. However, it may be relatively easy to create a trapped-like or counterstreaming electron population with magnetosheath energies on open field lines [*Fuselier et al.*, 1995]: the approximate balance of a field-aligned electron fluxes may also be observed for electrons on open field lines that are mirrored at low altitudes [*Fuselier et al.*, 1997]. However, recently *Phan et al.* [2005] suggested that equal fluxes of the counterstreaming electron population at all energies are a signature of closed field lines inside the magnetosphere. Another convincing signature of closed topology is a presence of counterstreaming oxygen outflowing from both southern and northern hemispheres [*Fuselier et al.*, 2001].

[12] The second complication is related to the definition of the magnetopause during northward IMF. According to the basic definition, the magnetopause is the current layer which separates the magnetospheric and magnetosheath plasma. During southward IMF, the magnetopause is easily identified by a major rotation of the magnetic field from the local magnetosheath to the magnetospheric orientation. However, under northward IMF, the orientation of both magnetic fields at the dayside will be similar and thus this observational identification becomes hard to perform. The difficulties in the recognition of the magnetopause were discussed by *Paschmann et al.* [1993]. They showed that under northward IMF, at the time when plasma temperature and distribution function undergo a rapid change there is almost no associated change in the magnetic field. It was pointed out [*Paschmann et al.*, 1993; *Song et al.*, 1993; *Fuselier et al.*, 1997] that for northward IMF conditions, the simple definition of the magnetopause as a current layer is not appropriate because there is no current present at a boundary separating two distinct magnetized plasmas with equal thermal pressure. It was suggested that the magnetopause be defined as a topological boundary separating the region in which magnetosheath population is dominant from that with significant presence of magnetospheric and ionospheric populations [*Paschmann et al.*, 1993]. One method for identifying this topological boundary for low magnetic shear situation involves the analysis of the electron temperature anisotropy [*Paschmann et al.*, 1993]. Magnetosheath electrons are nearly isotropic, but with $T_\perp > T_{II}$. However, heating at the magnetopause creates the opposite anisotropy, with $T_{II} > T_\perp$ [*Paschmann et al.*, 1993]. The dayside magnetopause during northward IMF may not provide conditions to effectively accelerate plasma populations observed inside the LLBL. However, *Onsager and Scudder* [2002] showed that some energization of the plasma populations is observed in situ at the high-latitude magnetopause where magnetic shear is sufficiently high. This can be either as a coherent acceleration, with little change in the temperature of the intermixing plasma components, or as a bulk heating [*Onsager and Scudder*, 2002]. The acceleration is due to the electric field component tangent to the magnetopause current layer [e.g., *Reiff et al.*, 1977]. The heating is observed in both electrons and ions and tends to increase the temperature in the direction parallel to the local magnetic field above that in the perpendicular direction.

[13] A third complication in the analysis of the boundary layer populations is the large and rapid backward and forward motions of the magnetopause and the LLBL. To analyze such cases, *Hapgood and Bryant* [1990, 1992] introduced the transition parameter (TP) technique for the reordering data inside the boundary layer. This is based on

the clear anticorrelation between electron density and temperature inside the boundary layer. Using the transition parameter, it is possible to reorder plasma and field data and remove the effects of the magnetopause and boundary layer motion from the data analysis. *Hapgood and Bryant* [1990] showed that inside the boundary layer there are always two distinct groups of data points: first, the section where electron density changes rapidly, but energy changes a little. This is adjacent to the magnetosheath population. The second group is where the energy changes rapidly, but the electron density changes only slowly. This is adjacent to the magnetospheric population. In a statistical study, *Hapgood and Bryant* [1992] showed that there is a smooth transition between the magnetosphere and magnetosheath states with many points representing plasma states intermediate between the two extremes if data are reordered according to the transition parameter. In all cases there are continuous traces between two extreme states without any abrupt changes, i.e., discontinuities, in the plasma. These observations gave them a reason to conclude that within the boundary layer there is a continuous change in the balance of processes controlling the transition between magnetosheath and magnetosphere.

[14] It is also possible to study the properties of the low-latitude boundary layer using satellite data from the cleft and cusp crossings, as magnetic field lines from the LLBL on the dayside maps into the relatively small area inside the cusp and cleft at low altitudes [e.g., *Newell and Meng*, 1988, 1992]. Midaltitude cusp crossings have been used to investigate properties of the electron edge of the LLBL during southward IMF [*Bogdanova et al.*, 2006]. The cusp region is populated by magnetosheath-like plasma which enters the magnetosphere via the reconnection process. Under southward IMF, plasma signatures of dayside reconnection in the cusp plasma population include plasma injections near the equatorward boundary of the cusp, antisunward convection, and "normal" energy-latitude dispersion with the plasma bulk energy decreasing with increasing latitude [e.g., *Smith and Lockwood*, 1996]. Under northward IMF, the signatures of plasma injections in the cusp from lobe reconnection include injections near the poleward boundary of the cusp, reverse, sunward plasma convection, and the opposite energy-latitude dispersion [e.g., *Crooker*, 1992; *Fuselier et al.*, 2000a; *Twitty et al.*, 2004]. In addition, it is possible to study dual-lobe reconnection processes using cusp observations [*Sandholt et al.*, 2000; *Provan et al.*, 2005; *Bogdanova et al.*, 2005, 2007]. The signatures of the dual lobe reconnection in the cusp observations include evidence of the counterstreaming oxygen ions [*Fuselier et al.*, 2001] and an existence of the more accelerated magnetosheath-like plasma [e.g., *Onsager et al.*, 2001; *Bogdanova et al.*, 2005]. However, some signatures of dual lobe reconnection inside the cusp are still not clear. For example, this process can be accompanied by strong sunward convection [e.g., *Sandholt et al.*, 2000; *Provan et al.*, 2005; *Bogdanova et al.*, 2007], while other studies argue that plasma on reclosed field lines is nearly stagnant [*Bogdanova et al.*, 2005; *Hu et al.*, 2008]. The expected nature of electron distributions is also unclear; *Phan et al.* [2005] suggested that a bidirectional electron population of the magnetosheath energies with balanced fluxes at all energies in the parallel and antiparallel direction is a signature of closed field lines. However, almost isotropic electron and ion populations have been observed on reclosed field lines inside the cusp [*Bogdanova et al.*, 2005]. This isotropization was explained as a result of pitch angle scattering. These different pitch angle distributions might be explained by the different "history" of field lines since reconnection: on newly closed field lines the population may be more bidirectional but becomes more isotropic with time due to pitch angle scattering.

[15] Thus, it is of interest to study the reconnection geometry and topology of the magnetic field lines which populated the LLBL near the dayside magnetopause and the LLBL(cleft)/cusp at low latitude during northward IMF using observations from satellites inside the cusp and near the dayside magnetopause. In this paper we present such observations, with Double Star TC1 close to the dayside magnetopause and crossing the LLBL as it moves backward and forward while Cluster is located inside the northern cleft/cusp region. We study in detail the structure of the LLBL near the subsolar point and the structure of the cusp/LLBL by examining high time resolution (4 s) magnetic field and plasma data. We also take into account the large-scale reconnection geometry which is revealed from SuperDARN data from both hemispheres.

[16] Using these simultaneous observations, we try to answer the questions: (1) What is the structure of the different sublayers observed inside the LLBL and cusp? (2) Can we simply map the LLBL observed near the dayside magnetopause into the cusp region? (3) How does the plasma population change as observed inside the LLBL near the magnetopause and inside the cusp at low altitudes? (4) How do the observed sublayers form?

[17] This paper is organized as follows: Section 2 gives a brief description of the Cluster, TC1, and ACE instruments used in this study; section 3 presents observations with subsection 3.1 showing the overview of Cluster and TC1 conjunction orbits and IMF conditions, subsection 3.2 showing SuperDARN observations in both hemispheres, subsection 3.3 showing the TC1 observations inside the dayside LLBL, and subsection 3.4 presenting the Cluster observations inside the cusp region. Section 4 contains a discussion and explanation of the observations with subsection 4.1 discussing TC1 observations, subsection 4.2 discussing Cluster observations and subsection 4.3 presenting a comparison of Cluster and TC1 observations. Finally, we present our conclusions in section 5.

2. Cluster, Double Star TC1, and ACE Orbit and Instrument Description

[18] This study is based on observations by the four Cluster satellites inside the midaltitude cusp region, by the Double Star TC1 satellite near the subsolar magnetopause, and by the ACE satellite in the upstream solar wind.

[19] The Cluster orbit has a perigee of $\sim$4 R_E and an apogee of $\sim$19.7 R_E, an inclination of $\sim$90°, and an orbital period of $\sim$57 h [*Escoubet et al.*, 2001]. The Cluster observations reported here were acquired by the Plasma Electron and Current Experiment (PEACE) [*Johnstone et al.*, 1997]. Each PEACE package consists of two sensors, HEEA (High Energy Electron Analyzer) and LEEA (Low Energy Electron Analyzer), mounted on diametrically op-

posite sides of the spacecraft. They are designed to measure the 3-D velocity distributions of electrons in the range of 0.6 eV to ~26 keV, with a time resolution of 4 s. In addition we used data obtained by the Hot Ion Analyzer (HIA) and Composition and Distribution Function (CODIF) sensors, which are parts of the Cluster Ion Spectrometry (CIS) experiment [*Rème et al.*, 2001]. These instruments are mounted on each of the Cluster satellites. The CODIF sensor combines a top hat analyzer with an instantaneous 360° field of view, with a time of flight section to measure the complete 3-D distribution functions of the major ion species: H^+, He^{++}, He^+, and O^+. The sensor covers the energy range between 0.02 and 38 keV/q with a time resolution of 4 s. The spacecraft potential is measured by the Electric Fields and Waves (EFW) instrument [*Gustafsson et al.*, 2001]. We also used magnetic field data from the Fluxgate Magnetometer (FGM) [*Balogh et al.*, 2001] with 4 s resolution.

[20] The Double Star TC1 satellite was launched in 2003 into an equatorial orbit at 28.2° inclination, with a perigee of 577 km, an apogee of 13.4 R_E, and an orbital period of 27.4 h [*Liu et al.*, 2005]. The orbit of the TC1 satellite is complimentary to the Cluster orbit, providing many possibilities for conjugated studies of magnetospheric dynamics. Some of the instruments on the TC1 satellite are similar to those on Cluster, and in this study we used data from the TC1 PEACE [*Fazakerley et al.*, 2005], CIS [*Rème et al.*, 2005], and FGM [*Carr et al.*, 2005] instruments. The data have been used with spin (4 s) resolution. The TC1 PEACE instrument consists of one sensor, which usually runs in alternating sweep preset mode. This means that every spin the sensor will cover different (high and low) energy ranges in alternation. The PEACE instrument on the TC1 spacecraft has enough telemetry for 3-D data to be available for every spin.

[21] ACE is orbiting the L1 libration point about 1.5 million km from the Earth and 148.5 million km from the Sun. The interplanetary magnetic field (IMF) data come from the Magnetic Field Experiment (MAG) [*Smith et al.*, 1998]. The level 2 data with 16-s resolution are used in this study. The solar wind density and velocity come from the Solar Wind Electron Proton Alpha Monitor (SWEPAM) [*McComas et al.*, 1998]; level 2 data with 64-s time resolution are also used. The solar wind dynamic pressure is calculated as $P_{sw} = N_{sw}\, m\, V_{sw}^2$, where N_{sw} is the solar wind density measured by ACE, m is a mass of proton, and V_{sw} is the solar wind velocity measured by ACE.

[22] The time lag associated with solar wind convection between the ACE, Cluster, and TC1 observations is calculated based on the X-component of the solar wind velocity, V_{Xsw}, in the GSE coordinate system (measured with a resolution of 64 s) and the position of ACE along Sun-Earth line (GSE x axis). The time lag is defined as $\Delta t = X/V_{Xsw}$, where X is the distance from ACE to the center of the Earth in the GSE X-direction. In the calculation of the time to the center of the Earth, we assume that the time taken for the shocked solar wind plasma to travel from the bow shock to the subsolar magnetopause through the magnetosheath is roughly equal to time needed for the normal solar wind to travel from the stand-off bow shock distance to the Earth (approximately 2–3 min [*Stubbs et al.*, 2004]). The appropriate solar wind velocity is calculated as the average velocity over a 20 min period around 45–65 min in advance of the Cluster and TC1 observations.

3. Observations

3.1. Overview of Cluster and TC1 Conjunction and IMF Conditions

[23] Figure 1 shows the Cluster and TC1 orbits during the time of interest, on 28 February 2004, 0000–0400 UT. The left plot presents a view of the projection onto the X-Z plane and the right plot shows a view of the X-Y plane in the GSM coordinate system. The magnetospheric magnetic field lines from the Tsyganenko T96 model are used [*Tsyganenko*, 1995] determined using parameters close to those observed. For Cluster, the tetrahedron configuration is shown scaled up by a factor of 20. During the time of interest the Cluster satellites are in the northern hemisphere and move from the nightside to the dayside via the mid-altitude cusp region. According to the T96 model, Cluster crosses the lobe sector, the cusp proper, and the dayside plasma sheet regions. The magnetic local time (MLT) of the Cluster satellites varies from 0940 at 0000 UT to 1209 at 0400 UT.

[24] At the same time, the TC1 satellite is near the subsolar magnetopause, and, according to the model predictions, moves from the magnetosheath into the dayside plasma sheet. TC1 is close to local noon, with a magnetic local time of 1234 at 0000 UT and of 1332 at 0400 UT. Thus, the difference between the Cluster and TC1 positions during the time of interest is in the range of 1–2 h of MLT with Cluster being slightly in the dawn sector and TC1 being slightly in the dusk sector. Thus, strictly speaking, the satellites are not on the same field lines. However, they are close to each other in MLT, and the inter-SC MLT difference (1–2 h) is small in comparison with previously estimated lengths of the X-line at the magnetopause, 6–11 R_E [e.g., *Chisham et al.*, 2004]. Thus, in this paper we consider nearly simultaneous measurements from the Cluster and Double Star TC1 spacecraft which might relate to each other. The closest predicted conjunction in time between these satellites is during the period when TC1 crosses the magnetopause near the subsolar point and the Cluster quartet is near the equatorward boundary of the cusp, moving from open to closed field lines.

[25] Figure 2 presents the solar wind and IMF conditions measured by the ACE satellite for the interval 27 February 2300 UT to 28 February 0300 UT. The ACE data have been shifted according to the estimated time lag of 56 min. The top three panels show the three components of the IMF in the GSM coordinate system. The fourth panel shows the IMF clock-angle, CA = $\tan^{-1}(B_Y/B_Z)$. The next two panels show the X-component of the solar wind velocity (GSE) and the dynamic pressure of the solar wind. The last panel shows the magnetopause stand-off distance calculated using the method of *Petrinec and Russell* [1995].

[26] During the time of interest the IMF B_X component is mostly negative and changes from ~0 nT at the beginning to −13 nT at the end. The IMF B_Y component is relatively low and varies around 0 nT in the range of ±5 nT. From 0220 UT B_Y increases, reaching 8 nT at 0300 UT. For most of the interval the IMF B_Z component is very strong and northward, ~10–14 nT. However, from ~0210 UT, B_Z

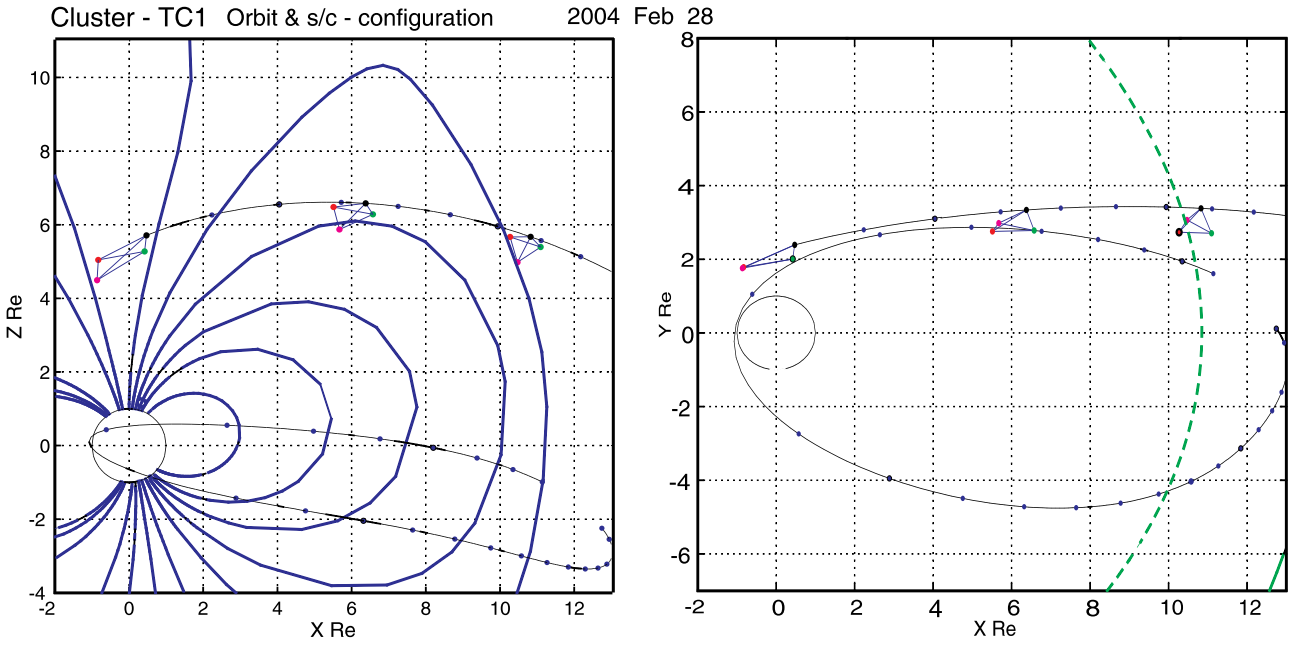

Figure 1. Cluster and TC-1 spacecraft tracks in the X-Z (left) and X-Y (right) plane in the GSM coordinate system between 0000 and 0400 UT on 28 February 2004. The orbit also shows the configuration of the Cluster spacecraft array as a tetrahedron (scaled by a factor of 20). The model geomagnetic field lines are shown for the projection into the X-Z plane and cut through the magnetopause is shown for the X-Y plane. The magnetospheric field lines are shown from the Tsyganenko T96 model based on observed external parameters.

decreases and becomes southward at ~0240 UT. The corresponding clock angle varies within the limits ±20° until ~0210 UT. At the end of the time of the interest, the clock angle increases and reaches 120° at 0300 UT.

[27] The solar wind velocity is relatively stable, $V_X \sim 420$ km s^{-1}. The dynamic pressure of the solar wind is slightly decreasing with time from 3.5 nPa at 2300 UT on 27 February to ~2 nPa at 0100 UT on 28 February. From 0100 UT, the dynamic pressure is relatively stable and exhibits small scale variations around an average value of ~2 nPa. The calculated stand-off distance varies in the range 9.5–10.5 R_E, and, in accord with the solar wind dynamic pressure, from 0100 UT exhibits small-scale variations with an amplitude of 0.2 R_E around an average position of 10.4 R_E.

[28] Figure 3 presents an overview of the electron data from the simultaneous observations by the Cluster and Double Star TC1 satellites on 28 February 2004, 0000–0340 UT studied in this paper. The first panel shows the electron energy time spectrogram measured at Cluster SC2. The black trace at the bottom of the panel represents the spacecraft potential. The second panel presents the electron energy-time spectrogram from TC1. On both panels, omni-directional differential energy flux (averaged over all pitch angles) is color-coded.

[29] At 0000 UT, SC2 is in the polar cap and detects low electron fluxes. At ~0035 UT SC2 starts to detect enhanced fluxes of a magnetosheath-like electron population and crosses some boundary layer near the poleward edge of the cusp. At 0040 UT SC2 enters the cusp proper, characterized by a strong enhancement of the fluxes of magnetosheath-like electrons with energies 30–500 eV. At ~0110 UT SC2 enters the boundary layer near the equatorward boundary of the cusp. This boundary layer is characterized by reduced fluxes of the magnetosheath-like electrons and by the appearance of low fluxes of electrons with plasma sheet energies, 1–10 keV. At ~0140 UT SC2 detects strong enhancement of the electrons with plasma sheet energies; however, until ~0200 UT, there are still some brief intervals of enhanced electron fluxes at low energies. From ~0200 UT SC2 enters the dayside plasma sheet proper, characterized by an electron population with energy 2–5 keV. An additional low-energy population, 10–40 eV, is of ionospheric or plasmaspheric origin. During the time of interest, the Cluster spacecraft separation is 200 km and the plasma populations observed by SC1, SC3, and SC4 are similar to SC2 during this crossing. The CIS instruments on all Cluster spacecraft have a data gap during the period 0040–0130 UT. Thus, we will significantly rely on PEACE observations.

[30] At 0000 UT TC1 is in the magnetosheath proper characterized by high fluxes of electrons with energies 15–200 eV. From ~0040 UT TC1 enters the plasma depletion layer (PDL) defined by the reduced fluxes and energies of the electron population [e.g., *Anderson and Fuselier*, 1993]. During the interval 0125–0200 UT TC1 crosses the boundary layer, which consists of accelerated magnetosheath electron population with energies 30–600 eV. This complicated crossing will be discussed in more detail later. At 0200 UT TC1 begins to detect high fluxes of the plasma sheet electron population with energies 1–20 keV. However, low fluxes of magnetosheath-like electrons are still detected. Thus, TC1 is inside another boundary layer. The energy of the magnetosheath-like population inside this

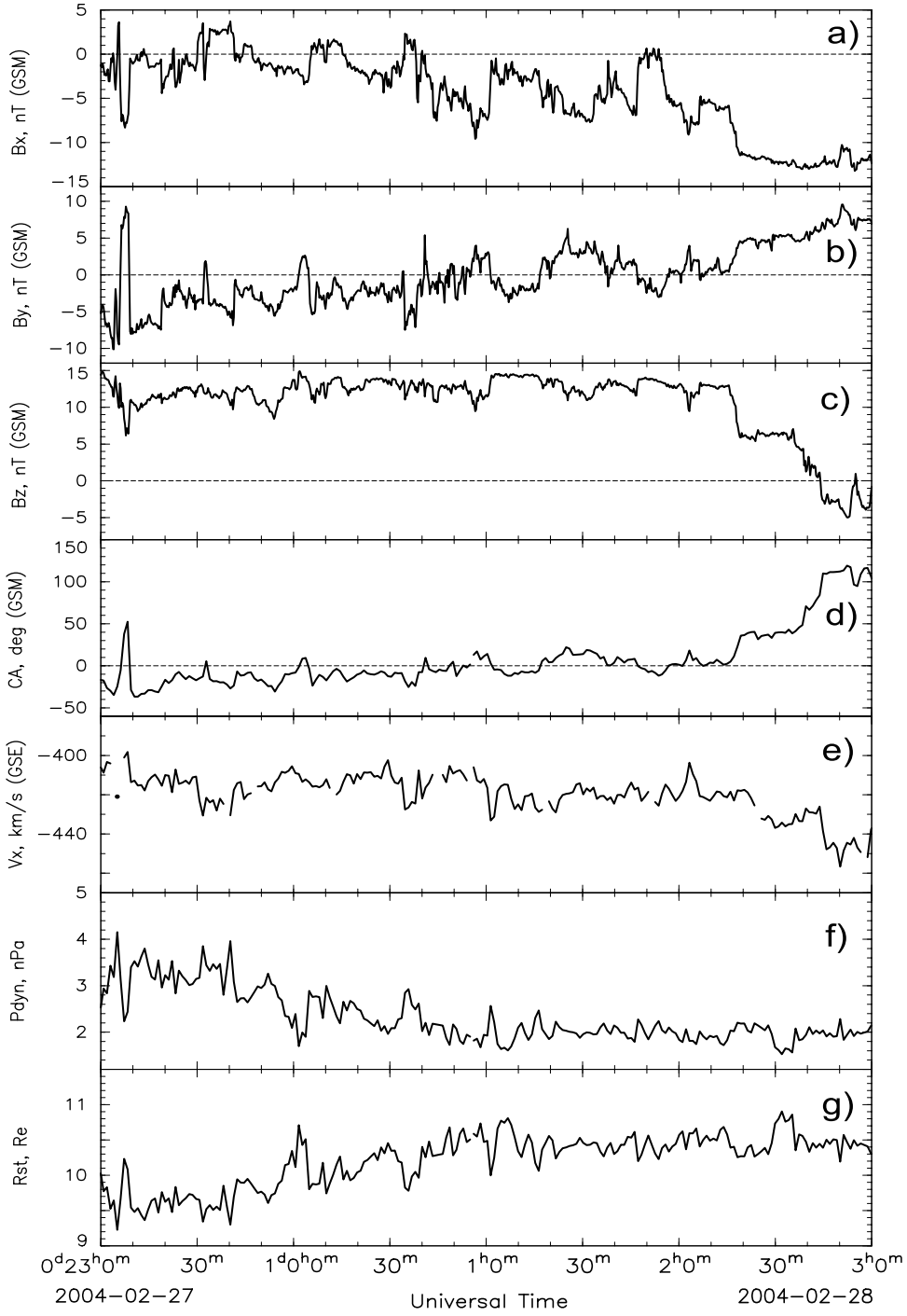

Figure 2. The IMF and solar wind conditions for the interval 27 February 2300 UT to 28 February 0300 UT. The top three panels show the X-, Y-, and Z-components of the IMF in the GSM coordinate system. The fourth panel presents the IMF clock-angle. The last three panels show the X-component of the solar wind velocity in the GSE coordinate system, the dynamic pressure of the solar wind and estimated stand-off distance of the magnetopause at the subsolar point. The ACE data have been shifted according to the estimated time lag of 56 min.

boundary layer is increasing with time. At 0320 UT the magnetosheath-like population disappears and at this time TC1 enters the dayside plasma sheet proper. Unfortunately there were some problems with CIS data transmission from TC1 during this time interval, and the transmitted CIS data are very noisy. Despite this, it is possible to observe ion populations similar to those described above inside different regions. However, inside the boundary layer with accelerated magnetosheath electron populations, low fluxes of ions with plasma sheet energies are observed among significant fluxes of ions with magnetosheath energies (not shown).

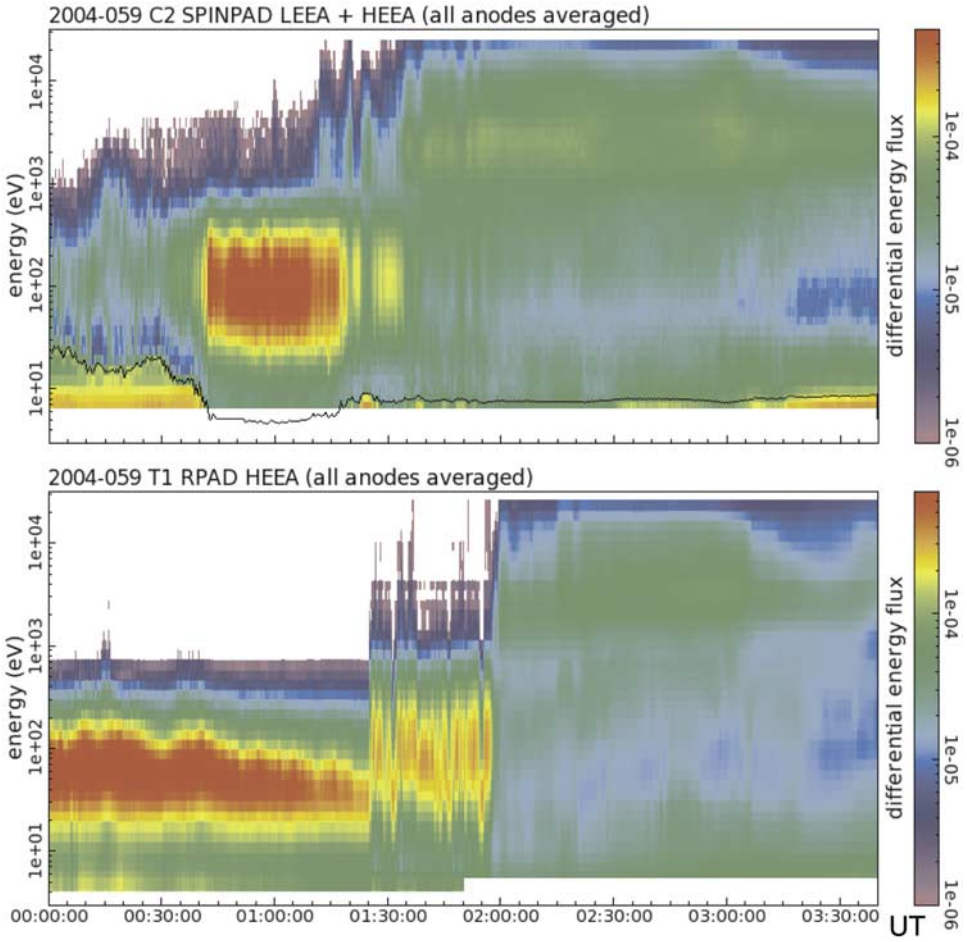

Figure 3. Overview of the nearly simultaneous observations from Cluster and Double Star TC1 satellite on 28 February 2004, 0000–0340 UT. The first panel shows the electron energy time spectrogram measured at Cluster SC2. The black line at the bottom of the panel represents the spacecraft potential. The second panel presents the electron energy-time spectrogram from TC1. On both panels, omnidirectional differential energy flux (averaged over all anodes) is color-coded.

[31] The closest conjunction in time between Cluster and TC1 is during the period 0125–0150 UT. During this time Cluster is near the poleward boundary of the cusp inside the boundary layer, and TC1 is inside the complicated boundary layer which contains an accelerated magnetosheath plasma population. The MLT difference between these satellites during this period is ~1 h. We note that as ion data are not available for the most of the time of interest, an analysis and interpretation of observations from the both Cluster and TC1 satellites will be based on electron and magnetic field data.

3.2. SuperDARN Observations in Both Hemispheres

[32] To estimate large-scale reconnection geometry, we investigate the ionospheric convection in both hemispheres using data from the Super-Dual Auroral Radar Network (SuperDARN) array of coherent scatter radars [*Chisham et al.*, 2007]. The SuperDARN radars measure the line-of-sight (l-o-s) Doppler velocity, spectral width, and the backscatter power from ionospheric plasma irregularities in 16 beam directions separated by 3.24° in azimuth. A full scan is completed in 2 min and covers 52° in azimuth and over 3000 km in range with a resolution of 45 km. Observations from different radars may be combined using the "map potential" technique [*Ruohoniemi and Baker*, 1998] in order to provide an estimate of the two-dimensional convection pattern in the high-latitude ionosphere. In this study we use the convection maps reconstructed from observations from nine radars in the northern hemisphere and four radars in the southern hemisphere.

[33] We studied the ionospheric convection at 10 min intervals for the period when Cluster crosses the cusp and TC1 crosses the boundary layer, 0040–0200 UT. Figure 4 presents a summary showing the convection maps in a magnetic local time/magnetic latitude coordinate system. On each map, dashed semicircles indicate parallels of constant magnetic latitude at 80°, 70°, and 60°. The radial lines indicate hours of magnetic local time with noon located at the top of the figure. Only the dayside part of the convection map is shown. On each map, locations of radar-derived velocity vectors of the ionospheric convection are represented by dots. The line attached to each dot indicates the convection velocity at that location derived by combining a line-of-sight radar measurement and an orthogonal component determined by the map potential

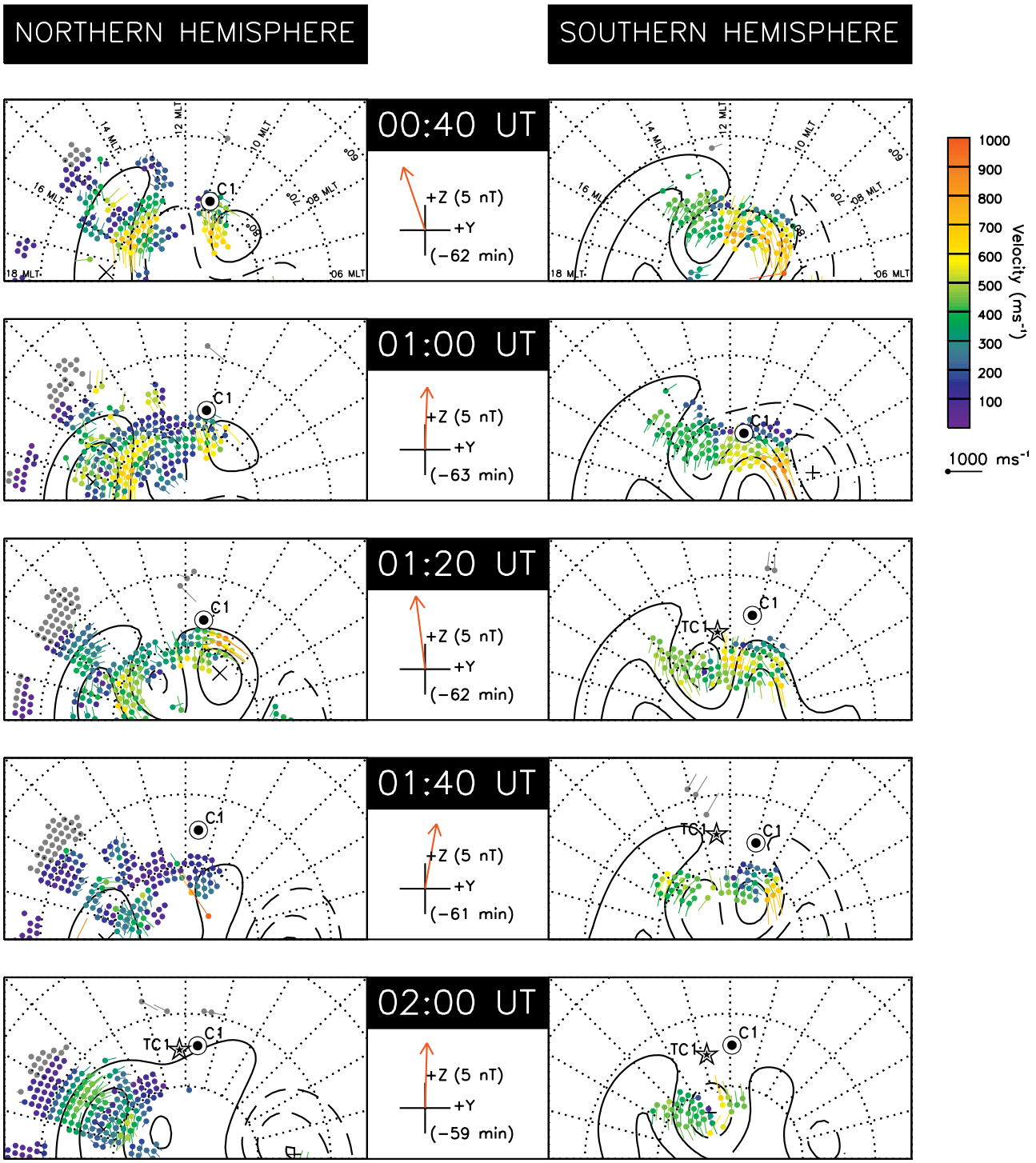

Figure 4. Streamlines and vectors of the ionospheric convection derived from SuperDARN observations of ionospheric flow in the northern (left column) and southern (right column) hemispheres during 28 February 2004. Convection maps are shown in the geomagnetic grid (MLT, ILAT) for five particular times during the period of interest. The circle and star represent Cluster and TC1 footprints respectively. The direction of the lagged IMF is shown at the center of each subpanel.

fitting technique. The magnitude of convection is indicated by color and by the length of the line. The black solid and dashed lines show equipotential lines which are predicted streamlines of ionospheric convection. The magnetic footprints of the SC1 and TC1 spacecraft are shown by star-shaped and circular symbols, respectively. Footprints are derived from the T96 magnetic field model [*Tsyganenko*, 1995] parameterized for the observed upstream solar wind conditions. The left and right columns show the convection maps in the northern hemisphere and southern hemispheres,

respectively, presented in a common coordinate system as if viewed from above the northern magnetic pole. The direction of the lagged IMF is shown at the center of each subpanel.

[34] The first row shows two convection maps at 0040 UT, when Cluster, in the northern hemisphere, enters the cusp region from the lobes. In the northern hemisphere, there is a convection cell in the dawn sector, with sunward flow at 11–12 MLT and return flow at lower latitudes. The predicted Cluster footprints are around 11 MLT, in the region of convection turning point from sunward to antisunward directions. In the dusk sector, a large convection cell is observed, with sunward convection at low latitudes turning to antisunward convection at higher latitudes, around 13 MLT. In the southern hemisphere, two-cell convection pattern is observed: there is sunward convection at 12 MLT, at the footprint of the cusp, and two return flows at lower latitudes in the dusk and dawn sectors. The sunward ionospheric convection inside the cusp, at around 12 MLT, corresponds to plasma injections from the reconnection site which is located poleward of the cusp, in the lobe sector. Thus, our observations indicate the existence of two reconnection sites: one site is in the lobe sector of the southern hemisphere and the second site is in the lobe sector of the northern hemisphere. Moreover, an additional reconnection site might exist at the dusk-lobe sector in the northern hemisphere. This reconnection site would drive the dusk convection cell in the northern hemisphere.

[35] The second row shows the convection maps at 0100 UT, when Cluster is inside the cusp proper and TC1 is still in the magnetosheath. The third row presents convection maps at 0120 UT, when Cluster enters the boundary layer near the equatorward boundary of the cusp and TC1 enters the boundary layer containing the accelerated magnetosheath population. For both intervals, the ionospheric convection is similar to the convection described above, at 0040 UT. It indicates that ionospheric convection and thus the reconnection geometry are stable over this period of 40 min. It is interesting to note that footprints of the Cluster spacecraft appear in the southern hemisphere at 0100 UT, indicating that according to the T96 model, Cluster is on closed field lines. At 0120 UT the TC1 footprints also registers in the southern hemisphere, again indicating that according the T96 model, TC1 should already be inside the magnetosphere.

[36] The fourth row presents the convection maps at 0140 UT, when Cluster is still inside the boundary layer near the equatorward boundary of the cusp and TC1 is inside the boundary layer near the subsolar magnetopause. In the northern hemisphere, the observed convection is much lower than before and almost stagnant: most of the convection vectors are around 100–200 m s^{-1} in comparison with 200–700 m s^{-1} during the previous interval. However, analysis still reveals two convection cells: one cell is in the dawn sector, with sunward, but very low, convection at 12 MLT, and the second convection cell is in the dusk sector. However, the Cluster satellite moves to lower latitudes and there are no observations of the plasma convection at the Cluster footprints. In the southern hemisphere, there are fewer measured convection vectors than before; however, the two-cell sunward convection pattern is still evident. There are no observations of the convection at the predicted footprints of both Cluster and TC1, which might indicate that both satellites moved out of the region with strong convection.

[37] The last row shows the convection maps at 0200 UT, when Cluster enters the dayside plasma sheet and TC1 crosses into the boundary layer populated by both plasma sheet and magnetosheath populations. In the northern hemisphere the convection cell at the dawn sector disappears, which indicates most likely the vanishing of the ionospheric plasma irregularities and thus no signal to reconstruct the convection. However, the convection cell at dusk still exists. Similar to the previous time interval, the footprints of both Cluster and TC1 are equatorward of the region with observed convection. There are only a few convection vectors in the southern hemisphere, and they indicate the existence of the sunward convection in the 11–12 MLT sector.

3.3. Analysis of the TC1 Observations

3.3.1. Overview of Boundary Layer Crossing by TC1

[38] An overview of TC1 observations on 28 February 2004, 0115–0210 UT is presented in Figure 5. Figure 5a consists of 10 subpanels. Each panel presents the pitch angle distribution (0°–180°) for electrons with center energy shown on the left (in the range 10–3800 eV). Differential energy flux is color-coded according to the logarithmic color bar shown on the right. Figures 5b, 5c, and 5d show the electron density, the electron temperature, and the anisotropy of the electron temperature, defined as $T_{II}/T_{\perp}$, respectively. Figures 5e, 5f, and 5g present the X-, Y-, and Z-components of the plasma (electron) velocity in the GSM coordinate system, respectively. The velocity time series are averaged over 40 s to remove short-scale fluctuations. Figures 5h–5k show the X-, Y-, and Z-components of the magnetic field in the GSM coordinate system and the magnitude of the magnetic field, respectively.

[39] At 0115 UT TC1 is in the plasma depletion layer, characterized by a depletion of the plasma density and an increase of the magnetic field strength compared to earlier magnetosheath values. The electron population inside the PDL is very anisotropic: the low-energy electron population, E $\sim$ 14–47 eV, moves antiparallel to the local magnetic field and the high-energy electron population, E $\sim$ 85–200 eV, moves parallel to the magnetic field. During the period 0115–0125 UT, when inside the PDL, TC1 detects a slight decrease of the electron density and very low temperature. The anisotropy of the electron temperature varies between 1 and 1.15. The measured plasma velocity is low, with the X- and Z- components close to zero. The Y-component of plasma velocity is around 100–150 km s^{-1}. Thus, the plasma in this region convects from the subsolar point toward the dusk sector. The magnetic field inside the PDL is quite strong, the magnitude of the magnetic field is $|B| \sim 80$–83 nT. The magnetic field is strongly northward, with the B_Z component being $\sim$80 nT, $B_X \sim 13$ nT and $B_Y \sim 0$ nT.

[40] At $\sim$0125 UT TC1 enters the boundary layer, characterized by energized magnetosheath-like electrons. It stays inside this boundary layer until $\sim$0158:00 UT, where the density is similar to that inside the PDL, $N_e \sim 9$–10 cm^{-3}. The electron temperature sharply increases in comparison to those inside the PDL, and stays at the same level throughout

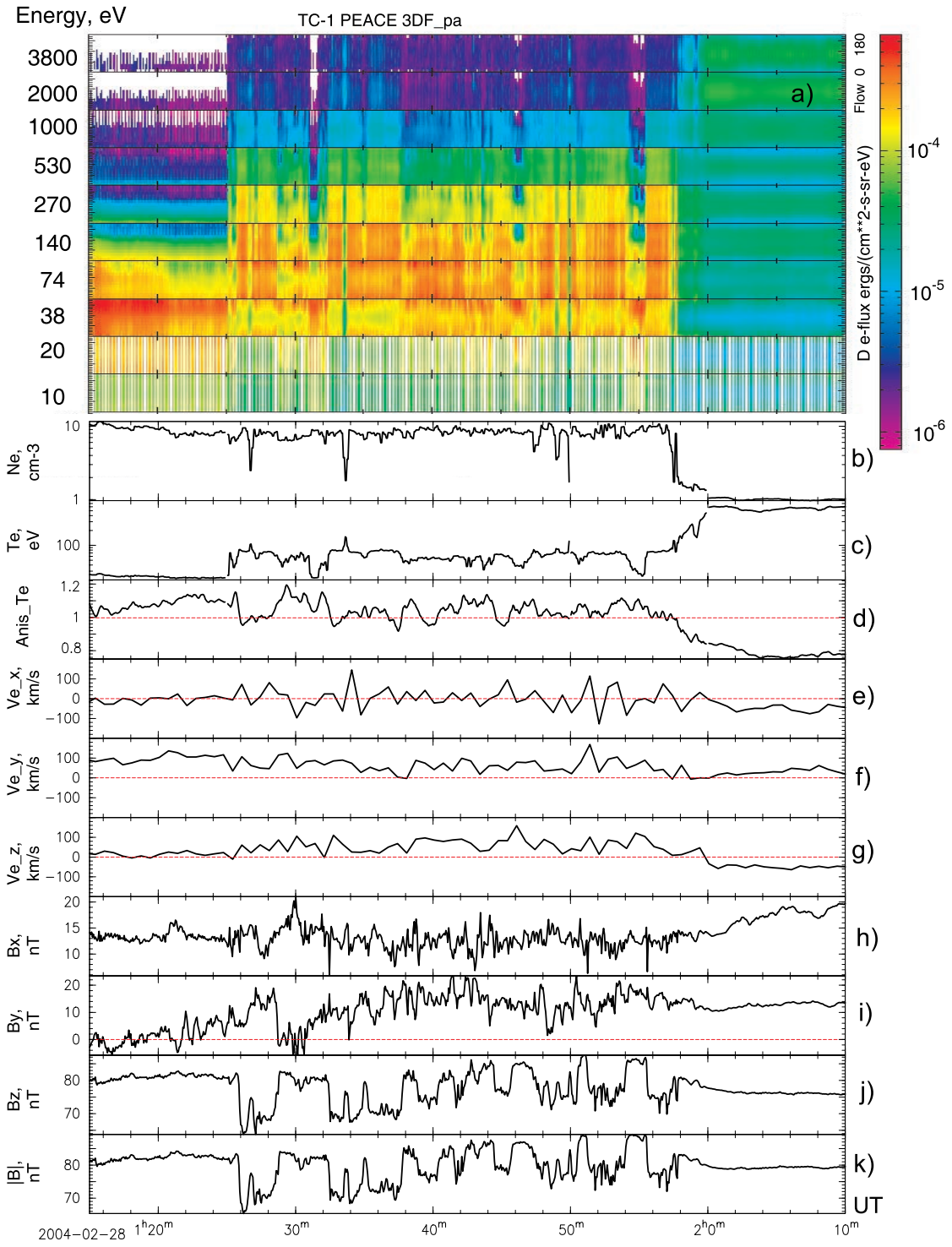

Figure 5. Overview of the TC1 observations on 28 February 2004, 0115–0210 UT. (a) Ten subpanels, in which each panel presents the pitch angle distribution (0°–180°) for electrons with center energy shown on the left (in the range 10–3800 eV). Differential energy flux is color-coded according to the logarithmic color bar shown on the right. (b, c, and d) The electron density, the electron temperature, and the anisotropy of the electron temperature, defined as $T_{II}/T_{\perp}$, respectively. (e, f, and g) The X-, Y-, and Z-components of the plasma (electron) velocity in the GSM coordinate system correspondingly. The velocity time series was averaged over 40 s to remove short-scale fluctuations. (h–k) The X-, Y-, and Z-components of the magnetic field in the GSM coordinate system and the magnitude of the magnetic field, respectively.

the boundary layer crossing, $T_e \sim 80-100$ eV. The anisotropy of the electron temperature varies within the limits 0.95–1.15. This crossing is characterized by enhanced variations in the X-component of the plasma velocity, $V_X \sim \pm 100$ km s^{-1}, by the Y-component of the velocity being similar to that inside the PDL, $V_Y \sim 60-100$ km s^{-1}, and by an enhanced Z-component, $V_Z \sim 30-100$ km s^{-1}. Thus, inside the boundary layer, the plasma moves duskward and northward. There are many small-scale variations in the X- and Y- components of the magnetic field inside this boundary layer, B_X varies in the limit $\sim$13 nT ± 3 nT, however, it stays almost at the same level as that inside the PDL. It is interesting to note that the direction of the X-component inside both PDL and boundary layer is in disagreement with that observed at ACE in the solar wind, changing from antisunward orientation inside the solar wind to sunward orientation inside the PDL and boundary layer, indicating significant draping of field lines inside the PDL. The B_Y component inside the boundary layer is within the limits $\sim$12 nT ± 5 nT. This component increases inside the boundary layer in comparison with the PDL value. When TC1 enters the boundary layer, the major changes happen in the B_Z component: B_Z decreases from $\sim$82 nT inside the PDL to $\sim$67 nT inside the boundary layer. The magnitude of the magnetic field inside the boundary layer is $\sim$70 nT.

[41] However, as one can see from variations in the magnetic field and electron pitch angle spectrogram, this boundary layer crossing during the period 0125:00–0158:00 UT is nonuniform. Thus, owing to the small-scale motion of the magnetopause, TC1 reenters the PDL at least three times: during the intervals $\sim$0131:00–0132:00 UT, $\sim$0145:30–0146:30 UT, and $\sim$0154:00–0155:30 UT. Each of these reenterings into the PDL is characterized by the electron population observed before in the PDL, by the reduction of the electron temperature and by the magnetic field values similar to the values observed before, inside the PDL. Additionally, analysis of the magnitude and the Z-component of the magnetic field shows that TC1 detects similar values of B_Z and $|B|$ to the PDL values during few short intervals at $\sim$0128:00–0131:00 UT, $\sim$0135:00 UT, $\sim$0137:00 UT, $\sim$0141:00 UT, and 0142:00–0144:00 UT. However, the electron population during these intervals is different to the PDL populations: the energy of the electrons varies in the range $E \sim 18-2900$ eV, and the population is more bi-directional: there are enhanced fluxes in the parallel and antiparallel directions. On the other hand, considering the electron population above 55 eV, one might see that the parallel fluxes of electrons are similar to those in the PDL, with antiparallel fluxes in addition. Thus, this population can be considered as a PDL population for the electrons in the parallel direction superimposed with a unidirectional (antiparallel) beam-like population. We will call parts of the boundary layer with such populations ''boundary sublayer with unidirectional electrons.''

[42] Apart from the previously discussed PDL electron population and population inside the sublayer with unidirectional electron beams, TC1 detects a third type of electron population inside this boundary layer during the intervals $\sim$0126–0128 UT, $\sim$0132–0133 UT, 0133:30–0137:30 UT, $\sim$0145:00 UT, $\sim$0147:00 UT, $\sim$0152–0154 UT, and $\sim$0156–0158 UT. This electron population is characterized by slightly more energetic electrons, by bidirectional electrons with energies 31–300 eV (however, fluxes of particles at 90° pitch angle also increase), and by significant fluxes of electrons with energies 300–5000 eV. There is a slight enhancement of electron fluxes at 90° pitch angle for this high-energy part of the electron population. Thus, these are signatures of mixing of the magnetosheath and plasma sheet populations on these field lines. We will call parts of the boundary layer with such populations ''boundary sublayer with mixing populations of bidirectional magnetosheath-like electrons and plasma sheet electrons.'' As one can see, there are multiple crossings by the TC1 spacecraft into different sublayers during this LLBL crossing, due to variations in the magnetopause stand-off distance.

[43] At 0158 UT, TC1 leaves the boundary layer characterized by accelerated magnetosheath-like electrons and enters into a fourth subcategory of boundary layer, characterized by a mixture of a plasma sheet-like electron population with enhanced fluxes at 90° pitch angle and a magnetosheath-like electron population with reduced fluxes. It is interesting to note that the low energy part of the magnetosheath-like population inside this boundary layer, $E \sim 14-85$ eV, is bidirectional, with enhanced fluxes at 0 and 180° pitch angles. However, the high energy part of the magnetosheath-like population, $E \sim 150-500$ eV, has enhanced fluxes at 90° pitch angle, i.e., is trapped. This boundary layer was observed for 2 min, 0158–0200 UT. During this time, the plasma properties change drastically: the electron density decreases from 9 cm^{-3} to 1–0.5 cm^{-3} (however, for some time, there is a ''plateau'' in the density), the electron temperature slowly increases from 100 eV to 700 eV, and the electron temperature anisotropy slowly decreases from 1 to 0.85. The velocity of the plasma changes as well and becomes smaller and stable. The magnetic field becomes more stable and closer to values observed later. We will call this boundary layer the ''transition layer.'' This transition layer is definitely on closed field lines, as indicated by existence of the plasma sheet trapped population.

[44] After 0200:00 UT TC1 enters the plasma region inside the magnetosphere with very stable plasma and magnetic field properties: the electron density is $Ne \sim 0.1$ cm^{-3}, the temperature is stable at $\sim$600–700 eV, the electron anisotropy is 0.7–0.8, and the velocity is steady with low antisunward and duskward components. The magnetic field inside this region is very stable with $B_X \sim 15-20$ nT, $B_Y \sim 10$ nT, and $B_Z \sim 75$ nT. However, this region still could not be considered as the plasma sheet proper, as it consists of a mixture of plasma sheet electron population and magnetosheath electron population, similar to observations inside the transition layer. Thus, we will call this region a ''boundary layer on closed field lines.''

[45] To summarize, during the interval 0115–0210 UT, the TC1 satellite crosses the complicated structure of back and forward moving boundary layers. Analyzing plasma and magnetic field data from TC1, we distinguish that TC1 crosses six different plasma regions during this time: a plasma depletion layer; a boundary layer with unidirectional electron beams, a boundary layer with accelerated magnetosheath-like population, which consists of two sublayers, with unidirectional and bidirectional electron populations

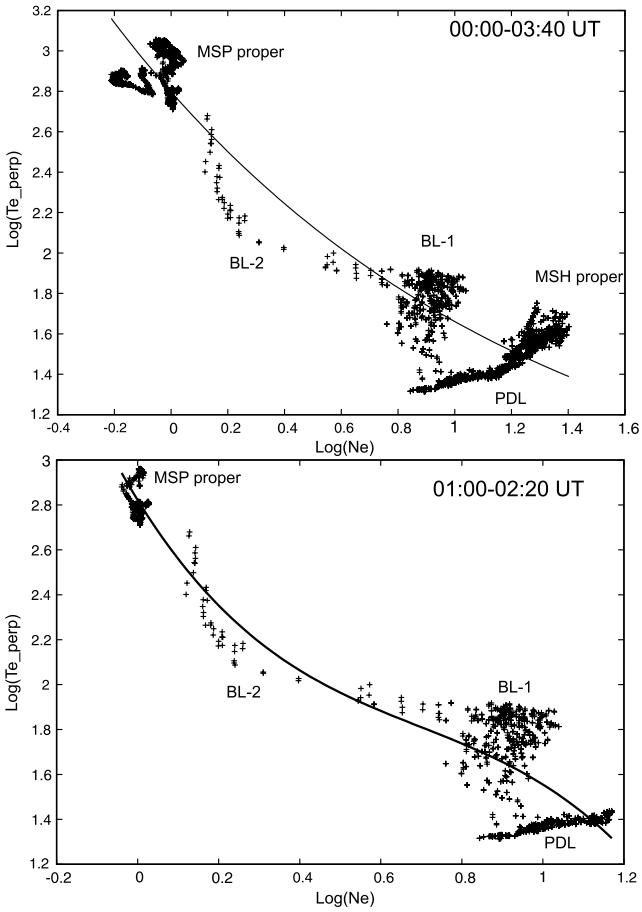

Figure 6. Scatter logarithmic plot of the electron density versus the electron temperature for (top) the interval 0000–0340 UT and (bottom) the interval 0100–0220 UT. The solid lines on both plots represent the least squares fits. On the top plot there are five groups of observational points, representing populations of the magnetosheath proper, the plasma depletion layer, two boundary layers, and the magnetosphere proper. On the bottom plot there are only four groups, the populations are similar to the bottom plot except the magnetosheath proper which is not observed due to a smaller time interval being used. The solid line on the bottom plot is used for the transition parameter reordering.

(with heated perpendicular population as well); a transition layer and a boundary layer on closed field lines.

3.3.2. Reordering of Crossing According to Transition Parameter

[46] To remove time variations in the crossing of the complicated structure of the boundary layers and emphasize the spatial variations, we reorganize data according to the transition parameter, using the ''transition parameter technique,'' introduced by *Hapgood and Bryant* [1992]. This technique is based on the anticorrelation between density and temperature of electrons inside the boundary layer. The transition parameter technique works well when there is a mixture of hot, tenuous plasma with cold, dense plasma, i.e., the magnetosphere and magnetosheath plasmas. However, in more complicated situation, when a third population is present (for example, an ionospheric population), this technique does not work. Thus, we carefully analyzed the electron population and removed the ionospheric population from the transition parameter analysis, calculating the partial moments (the electron density and temperature) inside the magnetosphere only for the population which includes plasma sheet and magnetosheath electrons.

[47] We establish the relationship between the electron density and temperature using scatterplots of $\log(N_e)$ versus $\log(T_e)$. The perpendicular temperature is used for the scatterplots. To find the transition parameter, corresponding to every observed data point, a best fit curve to the scatterplot of the electron density versus electron temperature during the crossing from the magnetosheath into the magnetosphere is determined. Each data point is then projected onto the curve by finding the point on the curve closest to the data point. Finally, a raw transition parameter corresponding to each data point is calculated by determination of the distance along the curve from the projected point to an arbitrary origin beyond the magnetosheath end of the distribution. The values of TP are normalized to be in the range from 0 to 100, such that TP = 0 corresponds to the magnetosheath population and TP = 100 corresponds to the magnetospheric population.

[48] Figure 6 presents two examples of scatter logarithmic plots of the electron density versus the electron perpendicular temperature, for the interval 0000–0340 UT (top) and the interval 0100–0220 UT (bottom). The solid lines on both plots represent the least squares fits. On the top plot, the population with $\log(N_e) \sim 1.2$–1.4 and $\log(T_e) \sim 1.5$–1.7 is the magnetosheath proper population, and the population with $\log(N_e) \sim 0.8$–1.2, and $\log(T_e) \sim 1.3$–1.5 is the plasma depletion layer population, plasma population characterized by a depletion in comparison to the magnetosheath. The cluster of points with $\log(N_e) \sim 0.8$–1 and $\log(T_e) \sim 1.4$–1.9 corresponds to observations inside the boundary layer with accelerated magnetosheath-like plasma. As we remember, inside this boundary layer the density of electrons was similar to the density inside the PDL and the temperature strongly increases. The population with decreasing density, $\log(N_e) \sim 0.8$–0.2, and increasing temperature $\log(T_e) \sim 1.9$–2.7, corresponds to the transition layer. Inside this layer, there is true anti-correlation between electron density and temperature. The cluster of points with low density, $\log(N_e) \sim 0.1$–0.2, and high temperature, $\log(N_e) \sim 2.7$–3, represents the boundary layer on closed field lines and the dayside plasma sheet proper. As one can see, there is a tendency of increasing temperature and decreasing density from the magnetosheath population toward the plasma sheet population. However, the relationship between electron density and temperature could not be described as smooth anticorrelation, as in the studies of *Hapgood and Bryant* [1992] and *Fear et al.* [2005a]. Moreover, the transition between the PDL population into the boundary layer with accelerated magnetosheath-like electron population is steplike, the temperature changes without significant change in density. As a result, we cannot find a good fit using a simple polynomial curve to describe the transition between magnetosheath and plasma sheet across the complicated structure of boundary layers.

[49] To improve this transition, we limit the time of interest to 0100–0220 UT (Figure 6, bottom). As one can see, we remove from our analysis the magnetosheath and

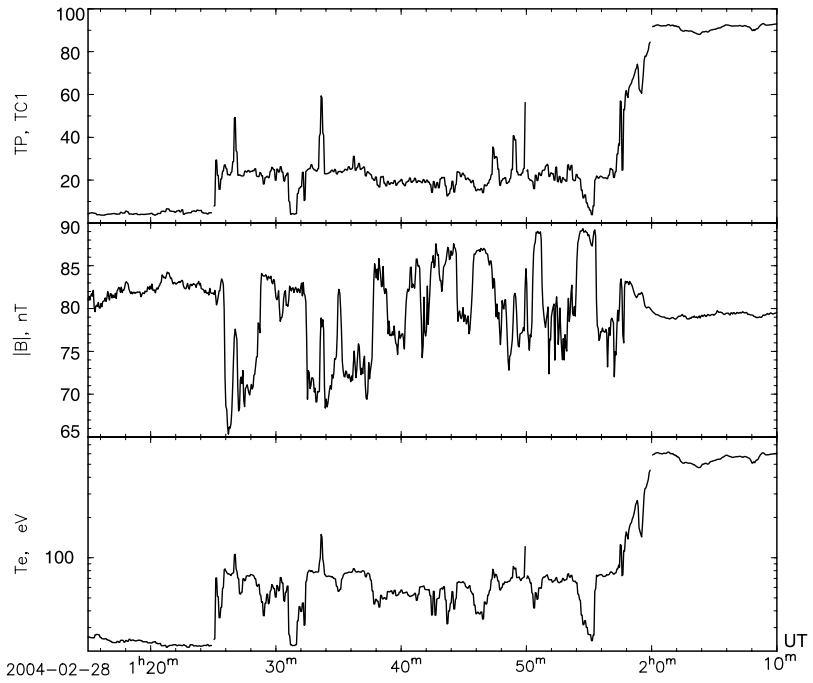

Figure 7. The transition parameter, the magnetic field magnitude, and average electron temperature versus time, the 28 February 2004, 0115–0210 UT, TC1.

plasma sheet proper populations. Thus, we now analyze the transition from the plasma depletion layer into the boundary layer on closed field lines across the boundary layers with accelerated magnetosheath-like electron population and the transition layer. The fitted curve shows relatively good anticorrelation between electron temperature and density and we use this curve for the estimation of transition parameter values, with the transition parameter TP = 0 being for the PDL population and the transition parameter TP = 100 being for the boundary layer on closed field lines population. Figure 7 shows results of the transition parameter estimations. The first panel presents the transition parameter and the second and third panels show the magnetic field magnitude and electron average temperature for the comparison. Inside the PDL, transition parameter is estimated to be between 0 and 7. Inside the boundary layer on closed field lines, from 0200 UT, the transition parameter is around 87–100. Inside the transition layer, during the interval 0158–0200 UT, the transition parameter varies in the limit from ~30 to 87. In the sublayer with unidirectional accelerated magnetosheath-like electrons, characterized by the magnetic field values similar to the PDL values, and by the electrons with average temperature of ~50 eV, higher than in the PDL, the transition parameter varies between 7 and 22. Finally, inside the sublayer with mixed populations of bidirectional magnetosheath-like electrons and plasma sheet electrons the transition parameter is estimated to be between ~22 and 30.

[50] Using the estimated transition parameter, we reorder the electron spectra across the complicated boundary layer structure. Figure 8 presents the results of this reordering, showing the electron energy versus transition parameter spectrogram for the antiparallel, perpendicular, and parallel differential energy flux (color-coded). The data are reordered over the period 0100–0220 UT. Now it is very easy to see the different boundary sublayers discussed above (marked by vertical dashed lines). Thus, the PDL is observed for TP = 0–7 and is characterized by antiparallel fluxes of electrons at low energies and parallel fluxes of electrons at higher energies.

[51] One can see that the interval with TP = 7–22, which corresponds to defined above boundary sublayer with unidirectional electron population, is not uniform and can be split into two subintervals according to the electron properties, with TP = 7–18 and TP = 18–22. During the period with TP = 7–18, there is a depletion in the fluxes of the perpendicular electron population. The fluxes of the parallel population are also less intense than before and during this interval there is continuous enhancement of the average energy of the parallel population. In the same TP range, TP = 7–18, there is also enhancement of the antiparallel fluxes at higher energies, $E \sim 80$–300 eV. However, the fluxes at these energies are low, and the population of the antiparallel electrons is still at energies ~50 eV. This could be a sublayer with a unidirectional electron population, as the parallel part of the population is similar to the PDL population, and the antiparallel part of the population is a new population with unidirectional electron beams. At TP = 18, the whole electron population drastically changes. First, there are enhanced perpendicular fluxes of the electrons with sharply increased energy, $E \sim 70$–300 eV. Second, the fluxes of the parallel population increase and this population becomes slightly more energetic, $E \sim 50$–300 eV. Finally, also at TP = 18, there is the start of a significant energization of the antiparallel electron population. During the interval with TP = 18–22, one can see a continuous energization of the antiparallel electron population, from average energy of 60 eV to ~100 eV. Similar, but less acceleration is seen in the perpendicular and parallel components. Analysis of the

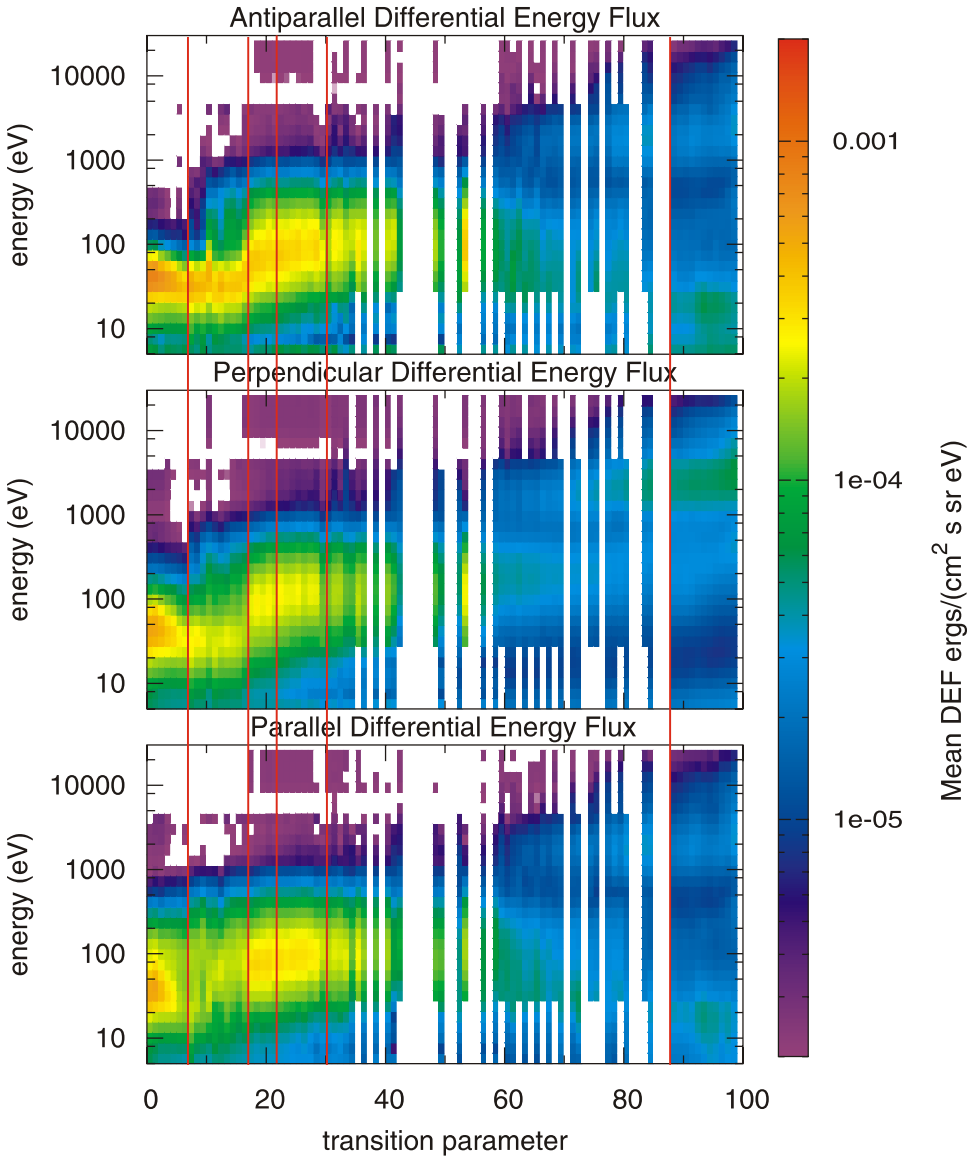

Figure 8. The electron energy-transition parameter spectrograms in the antiparallel, perpendicular, and parallel directions for the period of 28 February 2004, 0100–0220 UT. Differential energy flux is color-coded. The red vertical dashed lines mark different sublayers.

ratio of the differential energy fluxes of the population moving in the parallel to the magnetic field direction to that moving antiparallel (not shown) shows that the fluxes are not balanced at all energies. Moreover, the fluxes in the parallel and antiparallel directions are significantly larger than that in the perpendicular direction. Thus, this boundary sublayer can be described as a boundary layer with not balanced bidirectional electrons. We note that the discussed above unidirectional boundary layer is more complicated than we thought before and we now identify two sublayers: proper unidirectional sublayer with TP = 7–17 and sublayer with not balanced bidirectional electrons (TP = 18–22).

[52] During the interval with TP ~ 22–30, there are high fluxes of electrons with bulk population at 90–300 eV. This population is slightly more energetic than those observed during the interval with TP = 18–22. The electron fluxes are bidirectional with significant fluxes in the perpendicular direction as well. The ratio between fluxes in the parallel and antiparallel direction and that in the perpendicular direction is less than during the period with TP ~ 18–22. The energy of the electron population is stable over this TP range. There are some fluxes of the electrons with plasma sheet energies, E = 1–10 keV, but they are low. This high-energy population is more evident in Figure 5. According to Figure 7, the interval with TP ~ 22–30 corresponds to, for example, the time interval 0134–0138 UT. During this time, one can see some fluxes of electrons at energies 1–5 keV. The whole population is concentrated at TP = 22–30. Thus, this is the boundary sublayer with nearly balanced bidirectional energized magnetosheath-like electrons.

[53] During the range with TP = 30–87, the fluxes of the magnetosheath-like population are reduced, and we note that with increasing TP the energies of the parallel and

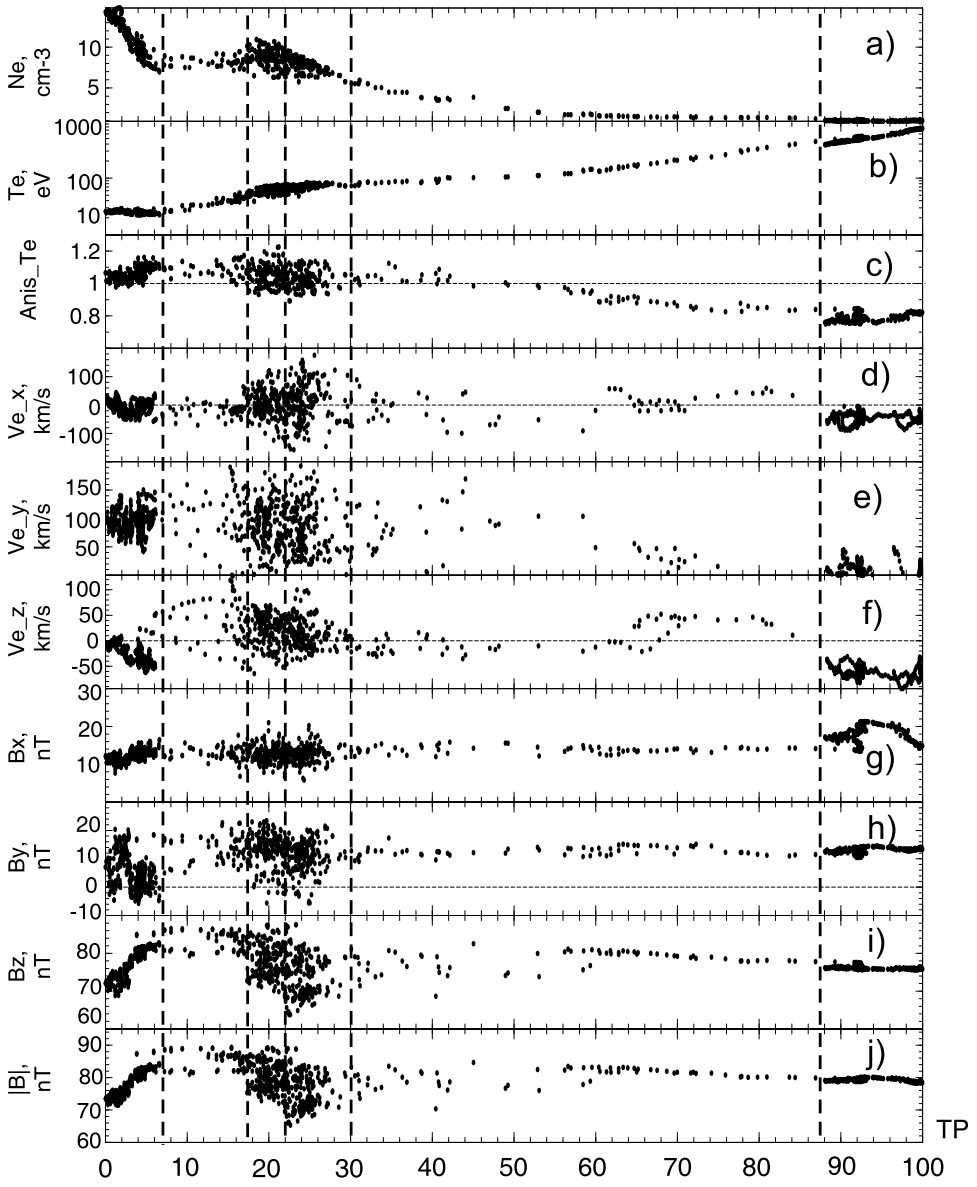

Figure 9. Overview of the LLBL crossing by TC1 on 28 February 2004, 0100–0220 UT. The plasma and magnetic field data are reordered according to the transition parameter. (a, b, and c) The electron density, the parallel electron temperature, and the anisotropy of the electron temperature. (d, e, and f) The X-, Y-, and Z-components of the plasma (electron) velocity in the GSM coordinate system, respectively. The velocity time series was averaged over 40 s to remove short-scale fluctuations. (g–j) The X-, Y-, and Z-components of the magnetic field in the GSM coordinate system and the magnitude of the magnetic field, respectively. The black dashed vertical lines mark different sublayers.

antiparallel components decrease. However, the energy of the perpendicular component slightly increases. During the same period low fluxes of plasma sheet electrons, E = 1–10 keV, are detected, mainly in the perpendicular direction. This is the transition layer.

[54] Finally, during the period with TP = 87–100, the fluxes of the plasma sheet population strongly increase while fluxes of the magnetosheath-like population decrease. We note that inside this layer the electrons with low-energy, E = 10–20 eV, are bidirectional. They are most likely of ionospheric or plasmaspheric origin. The magnetosheath-like electrons are concentrated at 90° pitch angle and there is some energy-TP dispersion: the energy of this population increases with increasing TP and at TP = 100 reaches energies of 800–900 eV. However, the fluxes of the magnetosheath-like population are low and are probably close to the one count level at the end of the interval. This magnetosheath-like electron population is obvious in Figure 5, during the time interval 0158–0210 UT. In Figure 7, one can see that the TP during this time interval is 87–95, which corresponds to a subregion discussed here. We define this region as the boundary layer on closed field lines. We note that the evolution of the electron population from the transition layer to the boundary layer on closed field lines as seen on the electron energy-transition parameter spectrogram is very smooth.

[55] We re-order the plasma moments and magnetic field data according to the transition parameter as well. Figure 9 presents results of this reordering, with the TP along the x axis. Panels, from the top to the bottom, show the electron density, the parallel electron temperature, the anisotropy of the electron temperature, the X-, Y-, Z- components of the plasma velocity in the GSM coordinate system, and the three components and the magnitude of the magnetic field (GSM). Similar to the previous plot, parameters were reordered over the time period 0100–0220 UT. To make presentation simpler, the dashed vertical lines separate the different plasma regions discussed above. As one can see, in agreement with the previous discussion, the PDL layer, with TP = 0–7, is characterized by decreasing electron density, N_e = 5–15 cm^{-3}, low (but stable) electron temperature, T_e = 20 eV, anisotropy of 1–1.15, duskward convection of plasma and by northward magnetic field.

[56] Inside the region with TP = 7–18, defined as the region populated by unidirectional magnetosheath-like electrons, the density is very stable, $N_e \sim 7$ cm^{-3}, the parallel electron temperature increases with increasing TP from 20 eV to 60–70 eV, and the anisotropy varies in the limit 1.1–1.2. The X-component of plasma convection is very low, $V_X \sim 0$ km s^{-1}, the V_Y component has a lot of scatter and varies in the limit 20–180 km s^{-1}, and the V_Z component is mostly positive, -40 km s^{-1} $< V_Z <$ 100 km s^{-1}. Inside this region, the X and Y components of the magnetic field are very steady with $B_X \sim$ 10–12 nT and $B_Y \sim$ 10–20 nT. The Z- component and the magnitude of the magnetic field reaches maximal values and exceed values inside the PDL, with B_Z being 80–85 nT and $|B|$ being 80–90 nT.

[57] Inside the region with TP = 18–22, which we defined as the region with unbalanced fluxes of bidirectional magnetosheath-like electrons (with significant heating of whole electron population), lots of scatter is observed in all parameters, except the parallel electron temperature. Inside this region, the electron density varies within the limits 6–10 cm^{-3}, the parallel electron temperature slowly increases from 70 eV to 90 eV, and the anisotropy of the electron temperature is 0.9–1.2. All components of plasma velocity are highly scattered, with V_X varying in the limit ±120 km s^{-1}, V_Y in the limit 20–200 km s^{-1}, and V_Z in the limit ±60 km s^{-1}. The B_X component is relatively stable, 10–14 nT, and B_Y is scattered in the limit -10–+20 nT. Both the Z-component and the magnitude of the magnetic field have tendency to decrease inside this TP interval, having values closer to and slightly less than those inside the PDL.

[58] The region with TP = 22–30 is defined as the region with a bidirectional magnetosheath-like population which is mixed with some plasma of plasma sheet origin. Inside this subinterval, the electron density is almost constant (slightly decreasing), and the electron parallel temperature is slightly increasing. The behavior of the other parameters (except the Z-component and magnitude of the magnetic field) over the transition parameter range TP = 22–30 is similar to the behavior inside the range TP = 18–22. The B_Z component and the magnitude of the magnetic field continue to decrease inside this region, with B_Z being within the limits 65–80 nT and $|B|$ being within the limits 68–82 nT. Inside this region, the X and Y components of the magnetic field are ~10 nT. There are less fluctuations in the plasma velocity than before, with $V_X \sim 0$ km s^{-1}, $V_Y \sim$ 100 km s^{-1}, and $V_Z \sim 0$ km s^{-1}.

[59] The region with TP = 30–87 is defined as a transition layer, as we detect both high- and low-energy electron populations inside it. We note that there are only a few data points in this region. The electron density is monotonically decreasing from 5 cm^{-3} to 0.5 cm^{-3}, the electron parallel temperature is continuously increasing from 100 eV to ~500 eV, and the anisotropy of electron temperature is slowly decreasing from ~1 to 0.8, indicating domination of the perpendicular population. The plasma velocity is very low, and the magnetic field is very stable. Finally, at TP = 87–100, inside the boundary layer on closed field lines, the electron density is very low, the parallel temperature still increases, and the anisotropy of the electron temperature is 0.8, indicating domination of the trapped population. The plasma velocity changes inside this region, $V_X \sim -50$ km s^{-1}, $V_Y \sim 50$ km s^{-1}, and $V_Z \sim -50$ km s^{-1}. The magnetic field is very stable and strongly northward.

[60] To summarize the TC1 observations and the reordering of these observations according to the transition parameter, we can say that the transition between the PDL and the boundary layer on closed field lines is very complicated and the order of the transition is the PDL (TP = 0–7), the sublayer of the accelerated magnetosheath-like population with a new unidirectional electron population, moving antiparallel to the magnetic field lines (TP = 7–18), the sublayer of the accelerated magnetosheath-like population with unbalanced bi-directional electron population and additional heating of whole electron population (TP = 18–22), the sublayer with accelerated magnetosheath-like population with nearly balanced bidirectional electron beams and with a trace of the plasma sheet electrons (TP = 22–30), the transition layer, characterized by a mixture of both, magnetosheath-like (with reduced fluxes) and plasma sheath like populations and by changes in the plasma parameters (TP = 30–87), and the boundary layer on closed field lines, characterized by a mixture of plasma sheet and magnetosheath electrons, however without significant changes in the plasma parameters (TP = 87–100). As one can see, transitions between the different regions sometimes are smooth and the defined TP limits for different plasma regions are probably sometimes subjective. The exception is the transition between different plasma states which happens at TP = 18, when we observe simultaneous heating of the whole electron population.

[61] Figure 10 presents a summary of typical electron spectra inside the different plasma regions identified above. The first row shows 2-D cuts of the electron differential energy flux. The horizontal axis corresponds to the perpendicular speed and the vertical axis corresponds to the parallel component. The figures have been mirrored around $V = 0$ for readability. The second row shows 1-D cuts of the distribution in units of differential energy flux. Cuts are in the parallel, perpendicular and antiparallel directions. The black line corresponds to the cut at 0° pitch angle, the red line at 90° pitch angle, and the blue line at 180° pitch angle. The third row presents 1-D cuts of the distribution in phase space density units. Column 1 presents the electron distribution function inside the PDL, at 0122 UT. The low-

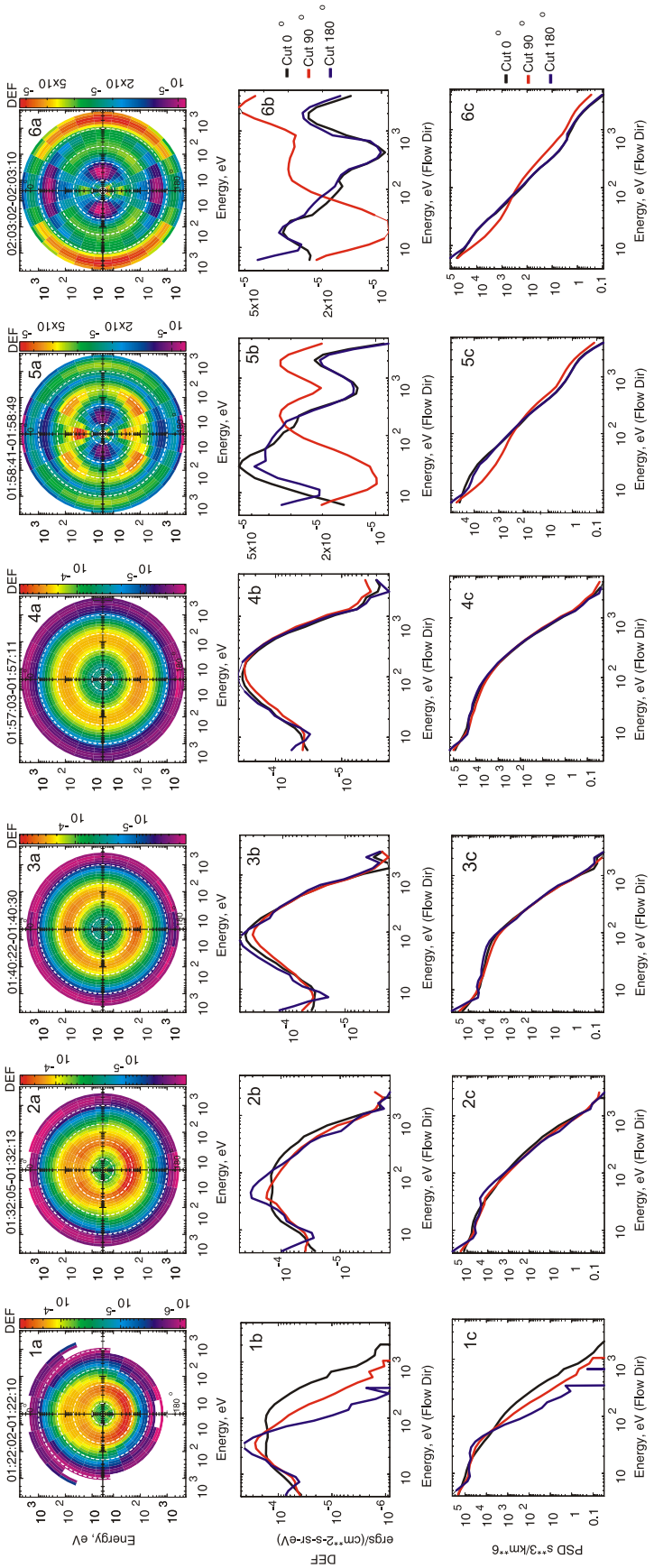

Figure 10. Electron distribution functions from the TC1 satellite. The first row shows 2-D cuts of the electron differential energy flux. The horizontal axis corresponds to the perpendicular (gyration) speed and the vertical axis corresponds to the parallel component. The figures have been mirrored around $V = 0$ for readability. The second row shows 1-D cuts of the distribution, in units of differential energy flux. Cuts are in the parallel, perpendicular, and antiparallel directions. The third row presents 1-D cuts of the distribution in phase space density units. The distribution functions are presented at times (1) ~0122 UT (inside the PDL), (2) 0132 (when unidirectional electron beam is detected), (3) 0140 UT (when significant heating is observed, but fluxes in the parallel and antiparallel directions are not completely balanced), (4) 0157 UT (when more heating is observed, and the counterstreaming population is balanced), (5) 0158 UT (inside the transition layer), and (6) 0203 UT (inside the boundary layer on closed field lines).

energy part of this population has strong fluxes in the antiparallel direction, while the high-energy population has significant fluxes in the parallel direction. Column 2 shows the electron distribution when unidirectional electron beams are detected, at ~0132 UT. The population at 0° pitch angle remains almost unchanged and is similar to the PDL population. However, the electron population is significantly heated and different to the PDL population. Column 3 presents the electron population inside the boundary layer with unbalanced bidirectional electrons, at 0140 UT, when significant heating occurs in all directions. One can see that fluxes of electrons in the parallel and antiparallel directions are not balanced at all energies. Column 4 illustrates the electron distribution inside the region with bidirectional electron population which mixes with the plasma sheet population, at 0157 UT. The population is more heated in comparison with the previous population; there is some slight increasing of the perpendicular component at high energies. The parallel and antiparallel electron populations are very close to being balanced at all energies. Column 5 presents the electron distribution function inside the transition layer, at 0158 UT. Inside this region, the electron spectra are very interesting and are observed for many spins. There are significant fluxes of the electrons with plasma sheet energies at 90° pitch angle. At low energies, there are observations of the bidirectional population. Moreover, the electrons with magnetosheath-like energies are dominant and they are concentrated at pitch angles of 45° and 135°. This might be a signature of strong pitch angle diffusion inside this region. Finally, column six shows electron spectra inside the boundary layer on closed field lines, at 0203 UT. At this time, the plasma sheet population becomes dominant, with enhanced fluxes at 90° pitch angle. The magnetosheath-like population still exists, and its fluxes also are concentrated in the perpendicular direction.

3.4. Analysis of the Cluster Observations

3.4.1. Cluster Observations Overview

[62] Figure 11 presents an overview of Cluster SC2 observations on 28 February 2004, 0020–0210 UT. Figure 11a consists of eight subpanels. Each subpanel presents the pitch angle spectrogram (0°–180°) for electrons with center energy shown on the left (in the range 8.3–3100 eV). Differential energy flux is color-coded according to the logarithmic color bar shown on the right. Figures 11b, 11c, and 11d show the electron density (logarithmic scale), the electron temperature (logarithmic scale), and the anisotropy of the electron temperature, defined as $T_{II}/T_{\perp}$, respectively. Different colors represent different Cluster spacecraft: SC1 is black, SC2 is red, SC3 is green, and SC4 is blue. Figures 11e, 11f, and 11g present the parallel and the X- and Y- components of the perpendicular plasma velocity in the GSM coordinate system, respectively. The velocity is calculated using PEACE 3DR data on SC2 (red) and HIA-CIS data on SC1 and SC3 (black and green lines). Unfortunately, there is a long data gap in the CIS observations during this interval, thus the ion velocity is plotted only when available. Figures 11h–11k show the X-, Y-, and Z-components of the magnetic field in the GSM coordinate system and the magnitude of the magnetic field, respectively. The Cluster color code has been used. There is a data gap in the FGM data during the interval 0045–0050 UT.

[63] At 0020 UT, Cluster is inside the polar cap characterized by low fluxes of particles. During the interval ~0033:00–0040:00 UT, Cluster detects low fluxes of the electrons with magnetosheath-like energies. These electrons are bidirectional. The electron density inside this region $N_e \sim 1–2$ cm^{-3}, the electron temperature is ~100 eV, and the anisotropy of the temperature varies in the limit 1.1–1.4. The parallel velocity increases up to 100 km s^{-1}. Strong convection is observed during this time interval, with $V_{\perp X}$ reaching −100 km s^{-1}, and $V_{\perp Y}$ reaching −50 km s^{-1}. Thus, the plasma convects antisunward and dawnward. This is in agreement with SuperDARN observations at this time in the northern hemisphere: the footprint of Cluster is near the "turning point" of the convection cell at the dawn sector. Small-scale variations are observed in the X- and Y-components of the magnetic field, and some depression of the X-component is also evident. We defined this region as a boundary layer near the poleward boundary of the cusp.

[64] During the period 0040–0047 UT, Cluster detects strong enhancement of the electron fluxes, and the density inside this region is ~10 cm^{-3}. The electron population is still strongly bidirectional at all energies, with fluxes in the parallel and antiparallel directions exceeding perpendicular fluxes. Analysis of the pitch angle spectrogram shows that fluxes at a pitch angle of 0° (downgoing population) are higher than at 180° (upgoing, mirroring population). The electron temperature decreases inside this region and is around 60 eV. There is a short data gap during this interval in the electron 3DR and magnetic field data, thus we are not able to make conclusions about plasma convection inside this region. This region we define as a cusp subregion with more bidirectional electron population.

[65] During the period 0047–0110 UT, the properties of the electron population inside the cusp change again: the electron population becomes more isotropic at energies 65–130 eV, with increasing fluxes in the perpendicular direction. However, the low-energy part of population, $E < 65$ eV, and the high-energy part of population, $130 < E < 580$ eV, show bidirectional beams. The electron population is not uniform and separate small duration injections are occurring, which will be discussed later. The density inside this region is 10–12 cm^{-3}, and the electron temperature is ~50 eV. The electron anisotropy is 1.2–1.3, and the plasma convection is very low, as is the parallel velocity. There are still some small-scale fluctuations of the X- and Y- components of the magnetic field inside this region. We defined this region as a cusp subregion with more isotropic electron population.

[66] Between 0110 and 0118 UT, Cluster encounters a new plasma region with different properties of the electron population. Magnetosheath-like electrons are observed with reduced fluxes in comparison to those during the previous time interval. These electrons become more bidirectional, with the maximum flux concentrating at 0–10° and 170–180° pitch angles. In addition, there are some fluxes of electrons with plasma sheet energies, $E \sim 1–3$ keV. These electrons have higher fluxes in the perpendicular direction. Thus, this is a boundary layer near the equatorward edge of the cusp on closed field lines. The density inside this layer is constant, $N_e \sim 8–9$ cm^{-3}, at the beginning and decreases

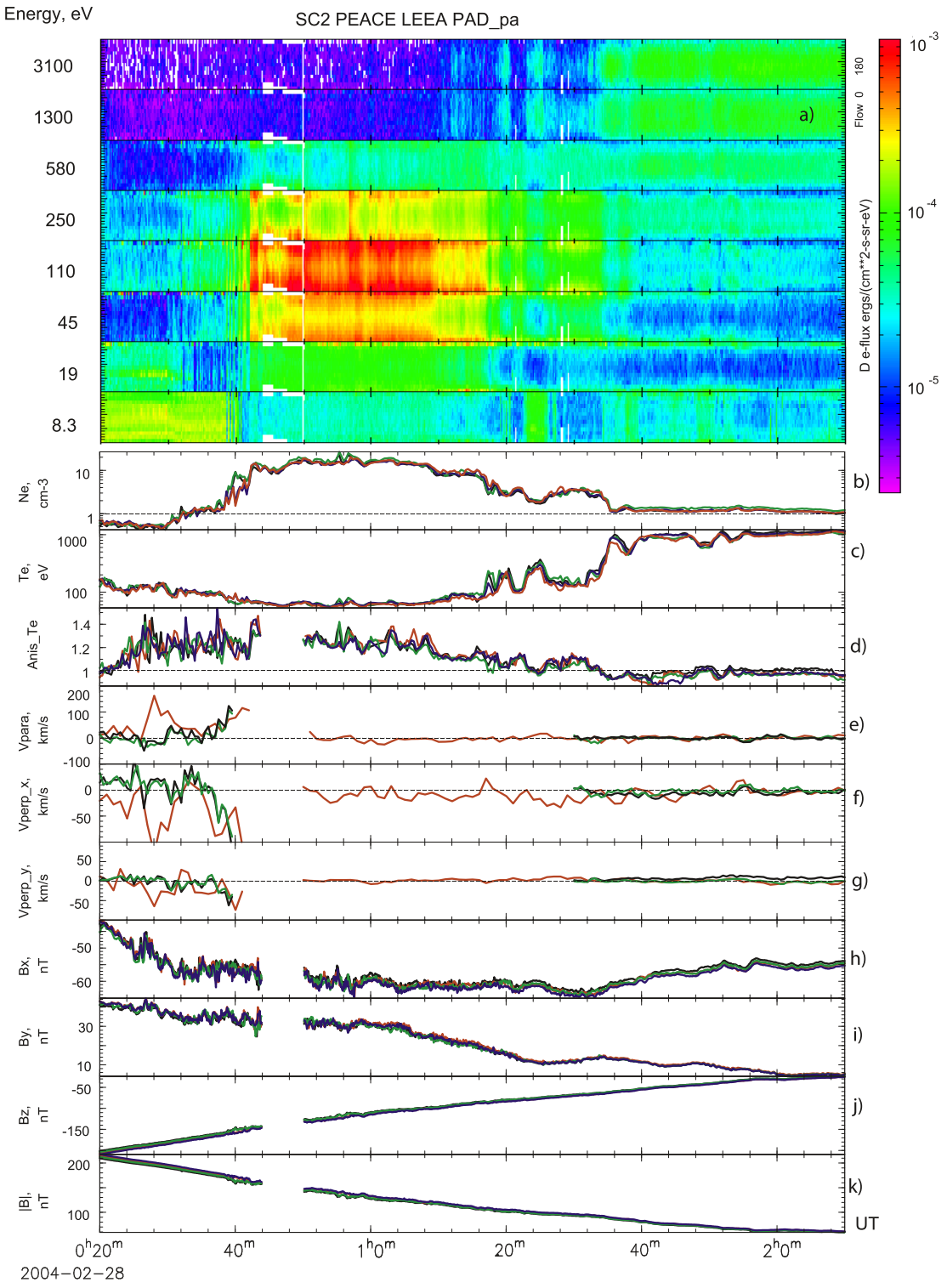

Figure 11. Overview of Cluster SC2 observations on 28 February 2004, 0020–0210 UT. (a) Eight subpanels, in which each subpanel presents the pitch angle spectrogram (0°–180°) for electrons with center energy shown on the left (in the range 8.3–3100 eV) Differential energy flux is color-coded according to the logarithmic color bar shown on the right. (b, c, and d) The electron density, the electron temperature, and the anisotropy of the electron temperature, defined as $T_{II}/T_{\perp}$, respectively. Different colors represent the different Cluster spacecraft: SC1 is black, SC2 is red, SC3 is green and SC4 is blue. (e, f, and g) The parallel and the X- and Y- components of the perpendicular plasma velocity in the GSM coordinate system, respectively. The velocity is calculated using PEACE 3DR data on SC2 (red) and HIA-CIS data on SC1 and SC3 (black and green lines). (h–k) The X-, Y-, and Z-components of the magnetic field in the GSM coordinate system and the magnitude of the magnetic field, respectively.

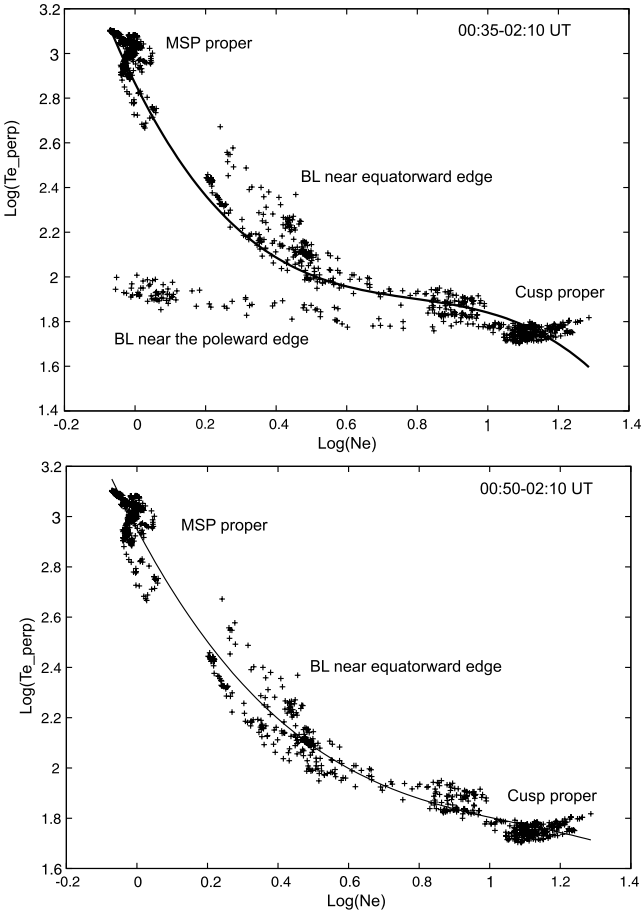

Figure 12. Scatter logarithmic plot of the electron density versus the electron perpendicular temperature for the intervals (top) 0035–0210 UT and (bottom) 0050–0210 UT. The electron data are from SC2, using the 3DR data product. The solid lines on both panels represent the least squares fits. On the top plot there are four groups of points, corresponding to the plasma populations inside: the cusp proper, the boundary layer near the equatorward edge of the cusp, the boundary layer near the poleward edge of the cusp, and the magnetosphere proper. On the bottom plot, the population inside the boundary layer near the poleward boundary of the cusp is removed.

slightly toward the end, $N_e \sim 5$ cm^{-3}. The electron temperature is increasing, $T_e \sim 90$ eV, and the anisotropy is around 1.1. However, this temperature anisotropy is averaged over the whole electron population, which consists of counterstreaming magnetosheath-like electrons and trapped plasma sheet electrons. The parallel and convection velocities are very low and there are less fluctuations of the magnetic field inside this region.

[67] Between 0118 and 0126 UT, the cusp appears to move backward and forward past the spacecraft twice, and this makes identification of different subregions inside and near the cusp more complicated. During the period 0126–0134 UT, Cluster crosses another sublayer which is characterized by an electron population similar to those inside the previous sublayer, during the interval 0110–0118 UT. However, fluxes of the magnetosheath-like electron population are greatly reduced. The electron density inside this sub-layer is constant and around $\sim$5 cm^{-3}, the electron temperature increases up to 150 eV, and the anisotropy $\sim$1. The plasma convection and parallel velocities are very low. It is hard to tell whether this region is an extension of the previously observed boundary sublayer on closed field lines near the equatorward edge of the cusp or if this is an additional boundary layer.

[68] Finally, at $\sim$0134 UT, Cluster enters a region characterized by strong enhancement of the plasma sheet electron population which is concentrated at 90° pitch angles. Inside this region, Cluster still detects low fluxes of the magnetosheath-like electrons. The low-energy part of these electrons, $E < 64$ eV, is bidirectional and the high-energy part, $130 < E < 490$ eV, has more flux at pitch angles $\sim$40° and $\sim$140°. The electron density inside this region is $N_e \sim 1$ cm^{-3}, and the electron temperature $T_e \sim 900$–1000 eV. The electron anisotropy becomes less than 1. The plasma velocity is very stable and low, and the magnetic field is very stable. Thus, this is another boundary layer on closed field lines near the equatorward edge of the cusp.

[69] As one can see, we find many subregions inside the cusp. To simplify analysis of Cluster observations and for the comparison with TC1 observations, we reorder Cluster observations using the transition parameter technique.

3.4.2. Reordering of Cluster Observations According to Transition Parameter

[70] First, as the transition parameter technique was introduced for the reordering the data for transition between the magnetosheath and the plasma sheet via the LLBL, we need to check if we can use this technique in the cusp region. Figure 12 shows two logarithmic scatterplots of the electron density versus the electron perpendicular temperature. Both plots are based on SC2 3DR data. Owing to telemetry available to the PEACE instrument on SC2, 3-D data is available with spin (4 s) resolution. For the top panel we use the time interval 0035–0210 UT, corresponding to the full cusp crossing from the boundary layer near the poleward cusp edge to the boundary layer near the equatorward cusp edge. On the scatterplot, we can identify four different clusters of points, corresponding to the cusp proper, two boundary layers, and the boundary layer on closed field lines near the equatorward edge of the cusp. Note that the electron population which corresponds to the boundary layer near the poleward edge of the cusp, with low density and temperature, is not very well fitted by the least squares curve. Thus, we cannot apply the transition parameter technique for the whole time interval. Therefore, we restrict the time interval to 0050–0210 UT (Figure 12, bottom). There is a very good anticorrelation between electron density and temperature over this time interval, and we use the estimated least squares fit for the transition parameter calculations. However, we should remember that we perform this estimation starting from 0050 UT, when Cluster is deep inside the cusp proper with more isotropic electrons. Thus, in our transition parameter analysis we will miss two subregions: the boundary layer near the poleward boundary of the cusp, and the beginning of the cusp, when bidirectional electron population is observed.

[71] Figure 13 shows the transition parameter estimation over the time of interest (bottom). Figure 13 (top) presents electron data from the PEACE LEEA sensor, for the

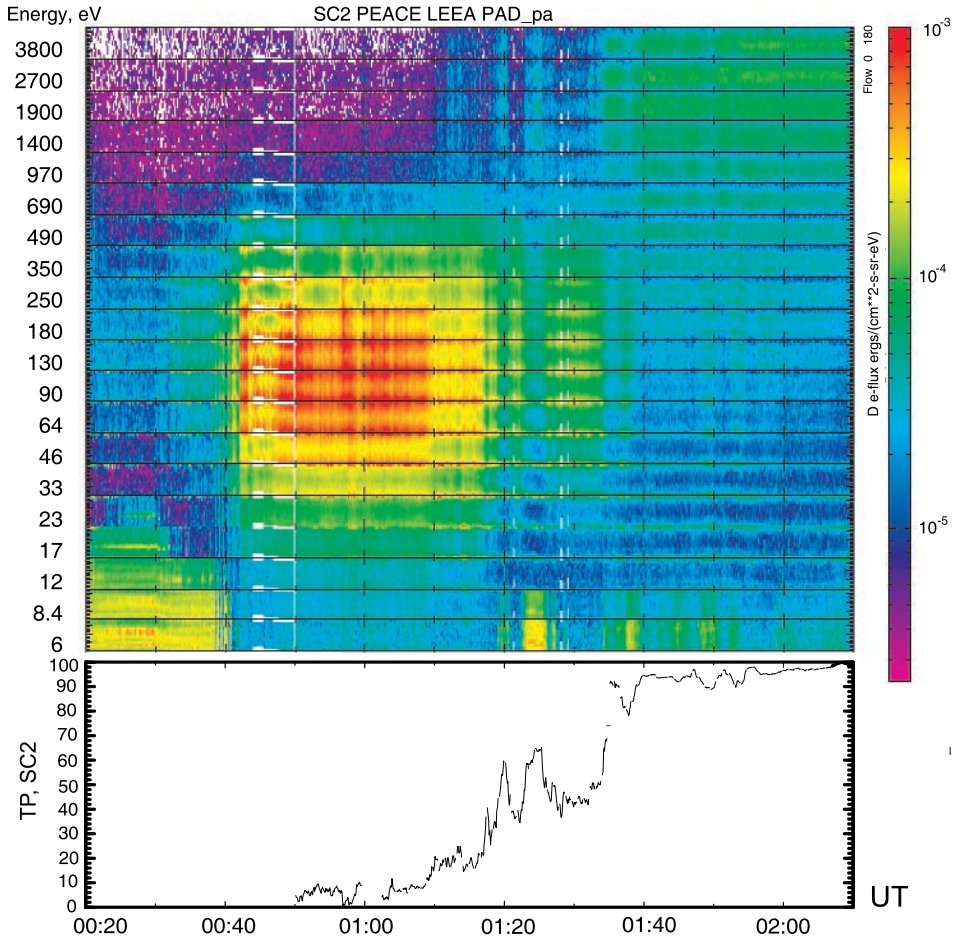

Figure 13. The top (colored) panel is electron data from the LEEA sensor of the PEACE instrument, on 28th February 2004, 0020–0210 UT, for 20 energy bins in the range 6–3800 eV. Each subpanel in the first panel presents the pitch angle distribution (0°–180°) for electrons with center energy shown on the left. Differential energy flux is color-coded according to the logarithmic color bar shown on the right. The bottom panel shows the transition parameter estimated from SC2 3DR data versus time.

comparison. Each subpanel shows the pitch angle distribution for electrons with center energy shown on the left. Twenty different energy ranges are used which allow us to see more details in the electron distribution. Thus, it is more clear that during the interval 0047–0110 UT, the electron population is not uniform, but small-scale separate injections are seen (especially at energy ranges of 180 eV and 250 eV) at ~0050 UT, ~0057 UT, ~0102 UT, and ~0103 UT. It is also clear that during the time interval 0047–0110 UT parallel and antiparallel fluxes of electrons are balanced at all energies, when compared to the electron distribution during the interval 0040–0047 UT, where the population with 0° pitch angle is dominant. This might suggest that during the period 0047–0110 UT the field lines are closed.

[72] The transition parameter during the period 0050–0110 UT, inside the cusp proper with more isotropic electron population, does not change much and varies in the limits 2–12. The transition parameter ~12–22 corresponds to the first boundary layer near the equatorward boundary of the cusp, observed during the period 0110–0118 UT. Most of the time, the TP is stable inside this layer and is around 20. During the interval 0127–0134 UT, inside the second boundary layer with similar electron population to those inside the previous boundary layer, but with reduced fluxes of the magnetosheath-like population, the transition parameter is in the range 35–50. Finally, during the period 0134–0210 UT, when Cluster is inside the third boundary layer near the equatorward boundary of the cusp, characterized by even more reduced fluxes of the magnetosheath-like population, the transition parameter varies within the limits 90–100.

[73] Figure 14 shows electron differential energy flux in the antiparallel, perpendicular and parallel directions reordered according to the transition parameter. Again, a similar time interval is used, 0050–0210 UT. Thus, TP = 0 corresponds to the cusp proper population with nearly isotropic electron distribution, and TP = 100 corresponds to the third boundary layer near the equatorward boundary of the cusp. The poleward boundary layer and beginning of the cusp proper is missing from this analysis. One can see that the reordered spectrogram shows very smooth transition of the electron spectra between the different regions defined above.

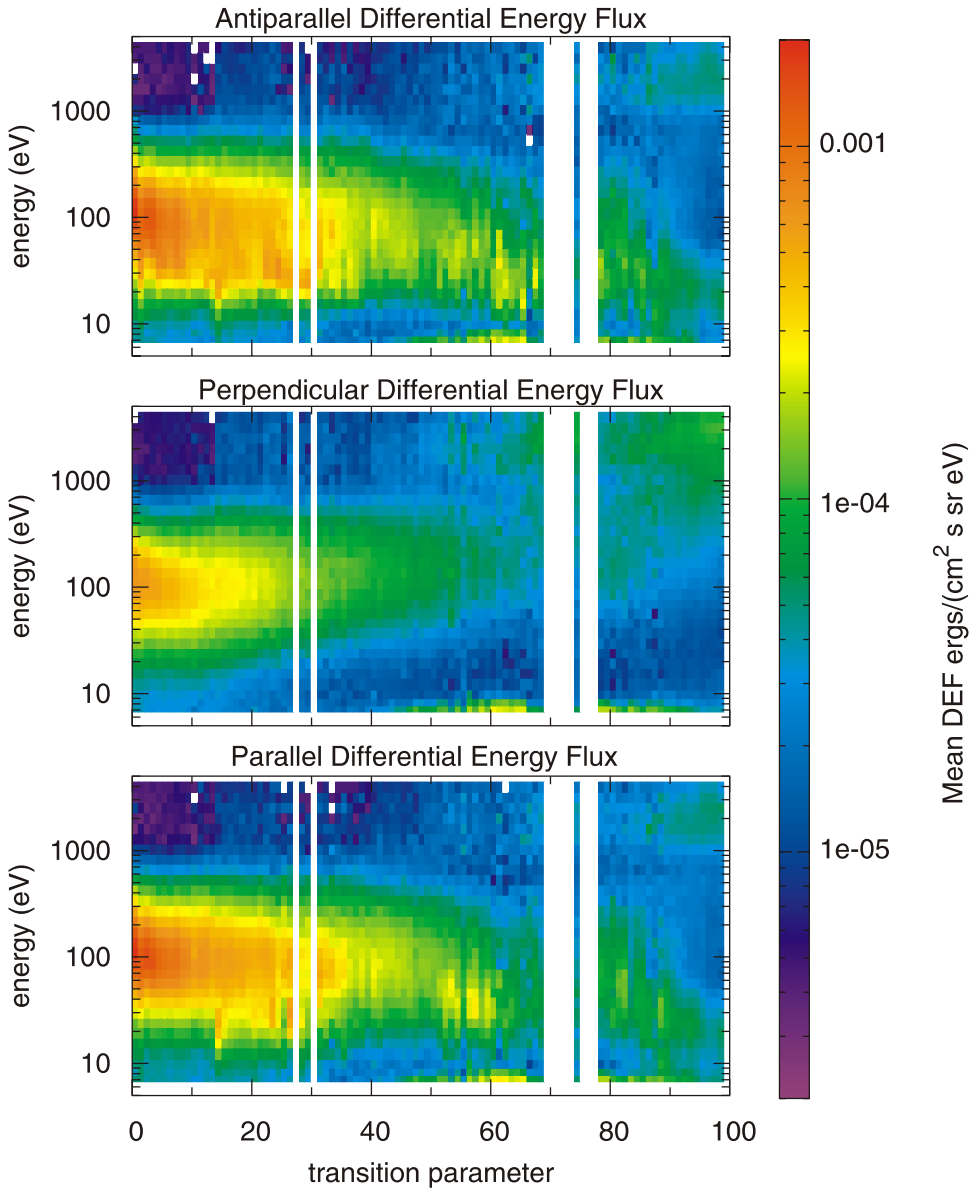

Figure 14. The electron energy-transition parameter spectrograms in the antiparallel, perpendicular, and parallel directions for the period of 28 February 2004, 0050–0210 UT, SC. Differential energy flux is color-coded.

[74] Thus, the fluxes of the magnetosheath-like electrons reduce with increasing TP. We note that the bulk energy of the parallel and antiparallel components of this population starts to decrease from TP $\sim$ 15, while the energy of the perpendicular component begins to increase from TP $\sim$ 15. At around the same TP, reduced fluxes of the plasma sheet electron population are detected, with more fluxes at 90° pitch angle. With increasing TP, the fluxes of the plasma sheet population become stronger. Speaking about the different subregions, one can note that during the period with TP = 0–12 (15), the fluxes of the magnetosheath-like electrons are very high with significant fluxes in the perpendicular direction (similar to observations presented in Figure 13). From TP $\sim$ 15, smooth changes in the electron population are observed, as mentioned above. The transitions between different sublayers are somewhat subjective, but we can conclude that during the period with TP = 15–100, three subregions are observed with more and more reduced fluxes of the magnetosheath-like electrons, corresponding to TP = 12 (15)–22, TP = 35–50, and TP = 50–100.

[75] Figure 15 shows the electron density, the electron parallel temperature, and the anisotropy of the electron temperature which are reordered according to the transition parameter. The transition parameter from SC2 is used, and different colors show data points from the different Cluster spacecraft (with the usual color code). This plot is reconstructed over the time interval 0050–0210 UT. There is a very good agreement between observations from all Cluster spacecraft. This figure clearly demonstrates that the transition from the cusp proper into the magnetosphere proper is smooth, with the electron density decreasing and the electron

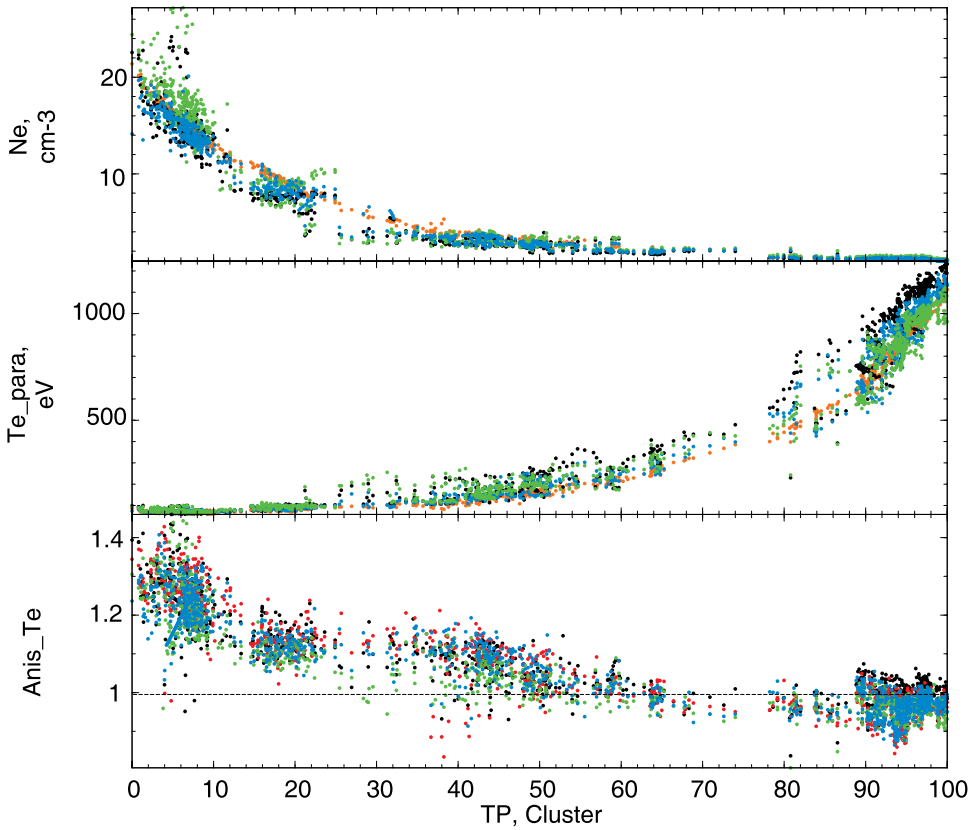

Figure 15. Overview of the cusp crossing by four Cluster spacecraft during the interval 0050–0210 UT. The electron density, the electron parallel temperature, and the anisotropy of the electron temperature are shown in the top, middle, and bottom panels, respectively. All parameters are reordered according to the transition parameter. The Cluster color-code is used.

temperature increasing with increasing TP. The anisotropy of the electron population is decreasing with the increasing TP as well, which indicates that the population is switching from being bidirectional at low energies to being trapped at high energies. However, one can see (especially on the density and anisotropy plots) that the electron population consists of four groups of points with a few points connecting these clusters. The first group of points, with TP = 0–10, corresponds to the cusp proper with more isotropic electron distribution. The electron density and anisotropy decrease across this region. The second group of points, near TP = 15–22, corresponds to the first boundary layer near the equatorward edge of the cusp. Inside this region, the electron parameters are stable and density plateau is observed at all Cluster spacecraft. The third cluster of points is concentrated near TP = 35–50. Inside this region, the density is relatively stable, but the temperature is increasing and the anisotropy of the temperature is decreasing. The fourth group of points is concentrated near TP = 90–100. Inside this group, there are prominent changes of electron parameters, with decreasing electron density and anisotropy and increasing temperature.

[76] Finally, Figure 16 presents examples of the electron spectra inside the different regions identified above. The format of this figure is similar to Figure 10. Column one shows the electron spectra at 0026 UT, inside the poleward boundary layer. As one can see, the electron flux is very low and the electron population is slightly bidirectional. This boundary layer might be the electron edge of the LLBL [e.g., *Bogdanova et al.*, 2006]. Column two presents the electron distribution inside the cusp subregion with more bidirectional electron population, at 0046 UT. Inside this region, electron fluxes are strongly increased. The electron distribution is strongly anisotropic, with parallel and antiparallel fluxes exceeding perpendicular fluxes and with parallel fluxes (downgoing population) exceeding the antiparallel fluxes (upgoing population). During this interval, there are missing data in the parallel direction, and thus we present cuts of the distribution at 20° and 160° pitch angles. Column three shows the electron distribution function inside the cusp proper with a more isotropic electron population, at 0055 UT. One can see significant heating of the whole electron population in comparison with the previous interval. However, fluxes of the counterstreaming population are still exceeding the fluxes of the perpendicular population. Moreover, the fluxes of the counterstreaming population are not balanced at all energies. Column four presents the electron distribution at ~0157 UT, inside the separate electron beam with slightly higher energies. The electron spectra are very similar to the previous interval, however, at this time the fluxes of the counterstreaming population are completely balanced, indicating that this population on closed field lines [e.g., *Phan et al.*, 2005]. Column five shows the electron spectra inside the first equatorward boundary layer, at 0116 UT. This boundary layer is dominated by the magnetosheath-like electron population which becomes more bidirectional in compari-

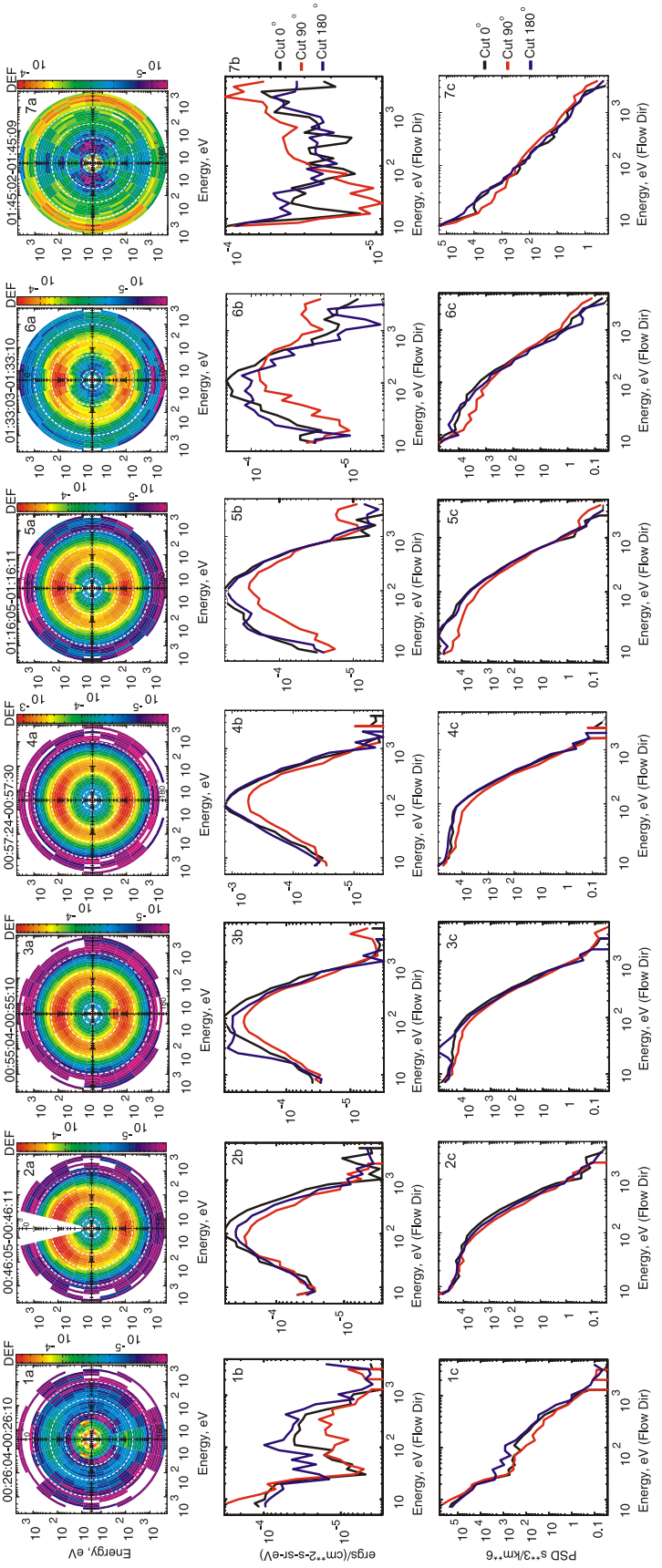

Figure 16. Electron distribution functions from the Cluster SC2 satellite. The format of the figure is similar to Figure 10. Distribution functions are presented at times (1) 0026 UT (inside the poleward boundary layer with reduced flux), (2) 0046 UT (inside the poleward boundary layer with bidirectional electron beams), (3) 0055 UT (inside the cusp proper with more isotropic electron population), (4) ~0157 UT (inside the cusp proper with isotropic population and balanced fluxes of the counterstreaming population at all energies), (5) 0116 UT (inside the first equatorward boundary layer), (6) 0132 UT (inside the second equatorward boundary layer), and (7) 0145 UT (inside the third boundary layer).

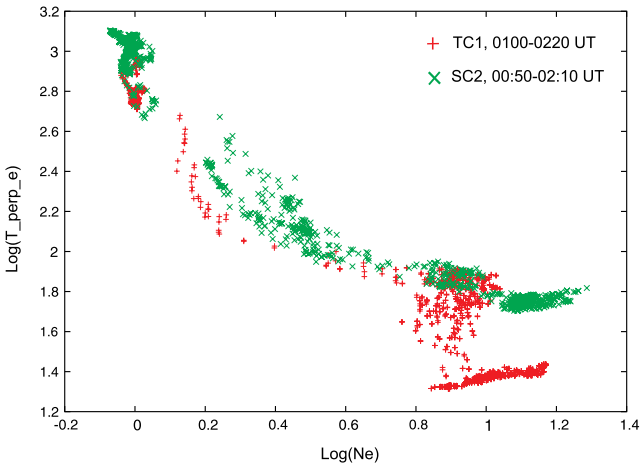

Figure 17. Comparison of Cluster and TC1 plasma populations. Scatter logarithmic plot of the electron density versus the electron perpendicular temperature. TC1 data is used for the interval 0100–0220 UT (red crosses). Cluster SC2 data is used for the interval 0050–0210 UT (green crosses).

son to that inside the cusp. However, the trapped plasma sheet population is also noticeable. Column six presents the electron distribution inside the second equatorward boundary layer. Inside this boundary layer, the plasma sheet population fluxes increase. Moreover, pitch angle diffusion of the magnetosheath-like population is observed, with particles at low energies being concentrated at 0° and 180° pitch angles and particles with higher energies having maximum fluxes at 45° and 135° pitch angles. Column seven shows the electron distribution inside the last boundary layer, at 0145 UT. Inside this region, the trapped plasma sheet is dominant and magnetosheath-like population is also trapped.

3.5. Comparison of Electron Populations Observed by Cluster and TC1

[77] Figure 17 shows comparison of Cluster and TC1 electron populations in the form of logarithmic scatterplot of the electron density versus electron perpendicular temperature. TC1 data is used for the interval 0100–0200 UT and Cluster SC2 data is used for the interval 0050–0210 UT. Recall that for Cluster we used the limited time interval, and points on the plot represent the cusp proper and three equatorward boundary layers. One can see that the Cluster and TC1 satellites detect similar plasma populations, especially those with high temperature and low density. This will be discussed further in section 4.

4. Discussion

4.1. Large-Scale Reconnection Geometry at the Magnetopause

[78] For the most of the time of interest the IMF is strongly northward and any antiparallel reconnection site is expected to be located poleward of the cusp, in the lobe sector [e.g., *Dungey*, 1963]. Moreover, these conditions are also favorable for the occurrence of dual lobe reconnection [*Song and Russell*, 1992; *Song et al.*, 2002]. As the IMF B_X component is negative, the reconnection is expected to happen first in the lobe sector of the northern hemisphere.

[79] The SuperDARN data presented in section 2 are in agreement with this suggestion. The SuperDARN observations of sunward ionospheric convection at the cusp footprints in both hemispheres reveal the existence of a reconnection site in the lobe sector of the southern hemisphere during the period 0040–0200 UT and the existence a reconnection site in the lobe sector of the northern hemisphere during the interval 0040–0140 UT. Simultaneous existence of reconnection sites in both lobes is suggestive that the process of dual lobe reconnection might occur for some time. Moreover, as sunward convection cells are observed over a period of 1 h, it suggests that both reconnection sites are continually in operation during the time of interest and that we can compare observations from the TC1 and Cluster satellites, even if they are not exactly at the same time. In addition, SuperDARN observations of the convection cell at the dusk sector of the northern hemisphere suggest the existence of an additional reconnection site at the dusk flank sector of the northern hemisphere during the entire time of interest. This additional reconnection site at the dusk flank sector makes observations more complicated and we must treat the nearly simultaneous observations between Cluster and TC1 with more caution, as they are separated by 1 h in MLT.

4.2. Discussion of TC1 Observations

[80] Our observations reveal that boundary layer crossing by TC1 was very complicated due to backward and forwards motion of the magnetopause, which is in agreement with the predicted stand-off distance of the magnetopause. Thus, we applied the transition parameter technique for this LLBL crossing. However, there is some disagreement in the reordering of the electron density and temperature during the transition between magnetosheath to plasma sheet populations across observed boundary layer in comparison to previous studies. *Hapgood and Bryant* [1992] show that there is a smooth transition between two extreme plasma states with many observational points corresponding to the transition states. In our data set, the transition between the PDL and LLBL populations is very sharp and seen only as a change in the electron temperature but not electron density. The smooth transition with increasing temperature and decreasing density is observed in our event for limited TP range, inside the transition layer. However, the whole transition was much more complicated than reported previously [*Hapgood and Bryant*, 1990, 1992]. Despite this, we show that it is possible to apply the transition parameter technique for the complicated boundary layers and that reordering data according the TP values is successful and reveals many important plasma (electron) features inside different sublayers of the LLBL.

[81] Using reordered (according to the TP) plasma and magnetic field data and analyzing the electron distribution functions, we conclude that TC1 crosses the different plasma regions which are formed by different processes. Figure 18 depicts all possible magnetic field topologies which are formed due to the dual lobe reconnection process. We suggest that the TC1 observations, while it moves from the magnetosheath into the magnetosphere, can be explained by TC1 crossing these different plasma sublayers

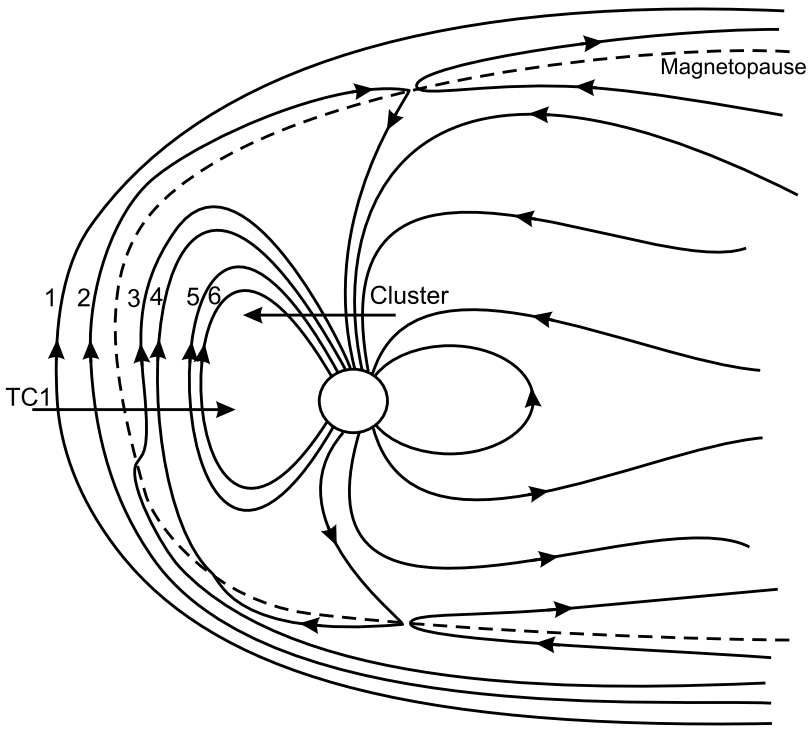

Figure 18. Schematic of the formation of the low-latitude boundary layer observed at the dayside by TC1 satellite. Line one shows the PDL field line, draped around the dayside magnetosphere. Line two represents a field line which is formed due to reconnection between the PDL and lobe field lines poleward of the cusp in the northern hemisphere. This field line is open and is outside the magnetopause, in the magnetosheath boundary layer. Line three represents an open field line which is formed due to reconnection poleward of the cusp in the northern hemisphere and which sinks inside the magnetosphere, crossing the magnetopause. Line four shows a field line which is formed by dual lobe reconnection. Line five represents field lines populated by plasma with reduced fluxes from both magnetosheath and magnetosphere sources. The process responsible for this population is diffusion across the magnetic field. Other lines show the magnetospheric field lines. The dashed line shows the magnetopause which is defined as a topological boundary.

The first region is the plasma depletion layer characterized by low plasma density and temperature and anisotropic electron population, with low-energy electrons moving anti-parallel to the magnetic field and high-energy electrons moving parallel to local magnetic field. These field lines are indicated by line one on Figure 18. The second region crossed by TC1 is populated by field lines with a specific electron distribution, where the parallel part of distribution is similar to the PDL population, and the antiparallel part is changed to the electron beam distribution over broad range of energies. These observations are similar to *Fuselier et al.* [1995, 1997]. These field lines are formed due to the reconnection process occurring between the draped magnetosheath (or PDL) field lines and lobe field lines poleward of the cusp in the northern hemisphere. These newly reconnected field lines are outside the magnetopause (line two on Figure 18). They contain the PDL electron population moving toward the reconnection site at 0° pitch angles and electrons heated at the reconnection site and propagating at 180° pitch angles.

[82] The next population sampled by TC1 is on field lines open during the northern lobe reconnection process which convect across the magnetopause, thus ''sinking'' inside the magnetosphere (line three in Figure 18). This sinking process links to the propagation of the kink in the magnetic field lines. As the magnetopause is a topological boundary, we suggest that the time when the spacecraft is crossing this boundary can be defined by the relative position of the spacecraft and the kink in the magnetic field. Thus, if the kink in the magnetic field is earthward relative to the spacecraft, it means that the satellite is located on the field line outside the magnetopause, in the magnetosheath boundary layer (line two in Figure 18). Alternatively, if the satellite is earthward relative to the kink in the magnetic field, it means that the kink passed over the spacecraft, and the satellite is located on the field lines which ''sink'' inside the magnetosphere (line three in Figure 18). In the TC1 observations, these field lines are marked by significant heating of whole electron population, not only in the parallel and antiparallel directions, but also in the perpendicular direction, similar to observations by *Paschmann et al.* [1993]. The transition from open field lines outside the magnetopause to the open field lines inside the magnetopause is very sharp on the data reordered according to the transition parameter, and it happens at TP = 17. In the reordered spectrogram, one can see a sharp increase in the energy of the electron population. A major rotation in the magnetic field is also happening around this TP value,

indicating that the kink in the magnetic field passed over TC1. The parallel and antiparallel fluxes of electrons on these field lines are not completely balanced, which indicates that these field lines are open [e.g., *Phan et al.*, 2005]. A heated electron population on open field lines inside the magnetosphere was observed previously by *Fuselier et al.* [1997]. During northward IMF, the magnetopause near the subsolar point is a topological boundary and thus we would not expect any heating to occur when the electron population is crossing this boundary. However, it was shown that significant heating of the plasma population might exist at the high-latitude magnetopause where shear between terrestrial and magnetosheath field lines is high [*Onsager and Scudder*, 2002]. As we established previously, the lobe reconnection was continuous during the time interval of interest, and we suggest that there is a continuous supply of reconnected field lines which slowly ''sinks'' inside the magnetosphere. When these field lines cross the magnetopause under high enough shear, the heated electron population is observed by TC1. Moreover, some energization may occur even at the low-latitude magnetopause, when the plasma population interacts with the kink in the magnetic field.

[83] The next population detected by TC1 is field lines reconnected a second time in the lobe sector of the southern hemisphere (line four on Figure 18). On these field lines, the magnetosheath-like part of the electron population undergoes additional heating which could be due to additional energization at the second reconnection site [*Onsager et al.*, 2001]. The parallel and antiparallel fluxes of the magnetosheath-like electrons are very close to being balanced inside this region. Moreover, the low fluxes of the electrons with plasma sheet energies indicate that these field lines are closed. This region is still dominated by the magnetosheath-like plasma and the electron density is still very high, being $\sim$6 cm^{-3}, and slightly decreases in comparison to that inside the boundary layer on open field lines, $N_e \sim 8$ cm^{-3}. Such a small change in the density of the plasma inside open and reclosed field lines is in agreement with previous observations by *Onsager et al.* [2001] and *Bogdanova et al.* [2005], but disagrees with observations by *Le et al.* [1996].

[84] For a short time TC1 samples the transition layer with unique plasma properties (line five on Figure 18). On this field lines, there is a strong reduction of the magnetosheath-like plasma flux in the comparison to the flux on the reclosed field lines. There are density and temperature gradients inside this region, which can indicate the cross-field diffusion due to wave-particle interactions [e.g., *Bauer et al.*, 2001]. In the diffusion process, the magnetosheath plasma enters the LLBL locally by scattering across the magnetic field lines. We can see indication of the diffusion probably in the electron distribution functions which show strong changes in the electron distribution according to pitch angles and some pitch angle scattering. Thus, we suggest that this boundary layer is formed by processes other than reconnection, most likely by diffusion process.

[85] Finally, TC1 enters the boundary layer on closed field lines characterized by a domination of the trapped plasma sheet population and by low fluxes of the trapped magnetosheath-like population (line six on Figure 18). This boundary layer probably is continuation of the transition layer and is formed during diffusion process inside the transition layer, as there is a constant change in the electron pitch angles inside these two layers from $\sim$45° and $\sim$135° inside the transition layer to 90° inside this boundary layer.

[86] In summary, we conclude that the LLBL observed by TC1 near the subsolar magnetopause has a complicated structure. Some parts of this boundary layer may be formed by single- and dual-lobe reconnection processes and some parts formed more likely due to diffusion processes. The observations and interpretation of the reconnection-formed part of the LLBL is similar to work by *Le et al.* [1996]. However, *Le et al.* [1996] based their observations and interpretation on ion data, and here we use electron data. Using high-resolution electron data and the transition-parameter re-ordering technique, we can identity two types of open field lines, inside and outside the magnetopause, which is different to the observations of *Le et al.* [1996]. Another disagreement is in the properties of the plasma on reclosed field lines. *Le et al.* [1996] showed examples where fluxes of magnetosheath and magnetospheric ion populations were comparable on the reclosed field lines and the plasma density was greatly reduced in comparison to that on open field lines. However, in the observations discussed here, the reclosed field lines are dominated by the magnetosheath-like plasma population and fluxes of electrons with plasma sheet energies are very low. Furthermore, the plasma density on reclosed field lines is only slightly reduced in comparison to that on open field lines. Thus, although our idea that part of the observed LLBL is formed by single- or dual-reconnection processes is similar to *Le et al.* [1996], the description of plasma signatures of closed field lines is different.

[87] Finally, we would like to discuss how our different subregions of the LLBL correspond to the outer and inner boundary layers discussed previously [e.g., *Bauer et al.*, 2001; *Song et al.*, 1990, 1993; *Le et al.*, 1996]. In the present event, the open field lines outside the magnetopause are the magnetosheath boundary layer [*Fuselier et al.*, 1995, 1997; *Onsager et al.*, 2001]. The outer boundary layer is characterized by mixing of both magnetosheath and plasma sheet populations and by the domination of the magnetosheath population [e.g., *Bauer et al.*, 2001]. Thus, the open field lines inside the magnetosphere and the reclosed field lines both correspond to the outer boundary layer. The inner boundary layer is characterized by equal fluxes of the magnetosheath bidirectional population and trapped plasma sheet population [e.g., *Song et al.*, 1993; *Bauer et al.*, 2001]. Thus, the inner boundary layer with properties described above was absent. In our event, however, an additional layer, which we call the transition layer, was observed. Inside this layer, the fluxes of the plasma sheet and magnetosheath populations were comparable, but magnetosheath-like electrons show fast changes in pitch angle from the counterstreaming population to the trapped population which we interpreted as a signature of enhanced diffusion inside this region.

4.3. Discussion of Cluster Observations

[88] The analysis of the plasma population inside the cusp reveals that the cusp observed by the Cluster satellites was surrounded by a number of distinct boundary layers. The first boundary layer is observed near the poleward edge of

the cusp and contains the reduced fluxes of electrons of magnetosheath energies. This boundary layer could be the electron edge of the LLBL. The electron edge of the LLBL is often observed in the midaltitude cusp crossings during southward IMF near the equatorward boundary of the cusp [*Bogdanova et al.*, 2006]. During northward IMF, when plasma inside the cusp is injected from the lobe reconnection site, the electron edge of the LLBL is expected to be observed near the poleward boundary of the cusp. Crossing into the cusp proper, Cluster observes strong convection and plasma injections with the parallel velocity $\sim$100 km s^{-1}. This indicates that plasma is injected from the reconnection site which is located poleward of the cusp in the northern hemisphere [e.g., *Fuselier et al.*, 2000b]. Thus, Cluster is on newly reconnected field lines which are characterized by significant fluxes of counterstreaming electrons. Deeper inside the cusp, SC2 detects a more isotropic population of electrons with significant heating of electrons at all pitch angles. The plasma inside this region is stagnant. However, the fluxes of the counterstreaming population at all energies are not completely balanced, indicating that these field lines are still open, despite the observed stagnation of the flow. Inside the cusp proper a few separate short-scale electron injections are observed. The electron energy inside these injections is slightly higher than energies observed before and after injections. Moreover, analysis of the electron distribution functions shows that fluxes of the counterstreaming population are balanced at all energies. These features in the electron population are both signatures of closed topology of the magnetic field lines [e.g., *Onsager et al.*, 2001; *Phan et al.*, 2005]. Thus, we conclude that these separate electron beams are on closed field lines which have been reclosed due to the reconnection process in the lobe sector of the southern hemisphere. Similar separate electron beams with higher energies are observed on the other Cluster spacecraft. Our observations imply that the second reconnection site is working in the pulsed regime, in agreement with previous observations by *Sandholt et al.* [2000], *Provan et al.* [2005], and *Bogdanova et al.* [2007].

[89] At $\sim$0110 UT, Cluster enters to the boundary layer characterized by bidirectional magnetosheath-like population which is mixed with the plasma sheet population. The magnetosheath-like population is dominant inside this region. This boundary layer is separated from the previous population by a sharp boundary. Inside this region, the plateaus in the electron density and temperature are observed, with density being around $\sim$8 cm^{-3} (in comparison to 10–20 cm^{-3} inside the cusp proper). Owing to existence of the plasma sheet trapped population, this boundary layer is on closed field lines. The plasma signatures are very similar to those inside the inner boundary layer near the magnetopause described in previous studies [*Bauer et al.*, 2001; *Le et al.*, 1996]. Owing to the observed density plateau, this boundary layer is more likely formed by the dual lobe reconnection process. It is possible that separate electron beams observed inside the cusp proper are on newly closed field lines. Thus, these field lines are not yet populated by the high-energy plasma. However, this boundary layer is on older closed field lines as hot magnetospheric population has had enough time for the drift onto them. The problem with this explanation is the sharp boundaries observed in the electron temperature and density when Cluster enters this boundary layer from the cusp. Alternative explanation of the formation of the inner boundary layer or "mixing region" was suggested by *Fujimoto et al.* [1998a]. They observed the mixing region near the tail flanks, where plasma properties were similar to those inside the IBL. Inside the mixing region, the plasma convects sunward. Thus, it was suggested that mixing of the magnetosheath and magnetospheric plasma occurs inside the mixing region farther down the tail and the solar wind particles in the mixing region might be supplied to the magnetosphere by the same process as those in the cold dense plasma sheet [*Fujimoto et al.*, 1998b]. In the present event, the plasma convection inside the boundary layer is slightly antisunward, $V_{\perp X} \sim -10$ km s^{-1}, but this is essentially zero giving the PEACE instrument error range. We should mention that the boundary layer described above is often observed in Cluster midaltitude cusp crossings during northward IMF, thus we need to study other events to confirm our conclusion about formation of this boundary layer.

[90] At $\sim$0118 UT, there is sharp transition into a different boundary layer. Inside this layer, the electron density decreases and the electron temperature increases. However, in the scatterplot (Figure 12) one can see that inside this layer there is a continuous change in these parameters, which is also seen in Figure 15. Thus, this may indicate that diffusion process plays an important role in the formation of this layer. The electron distribution functions show some pitch angle scattering, with increased fluxes at 45° and 135° pitch angles and decreased fluxes in the parallel and antiparallel direction. This may indicate that magnetosheath-like electrons continuously fill the loss cone and due to pitch angle diffusion are lost in the ionosphere [e.g., *Song et al.*, 1993].

[91] Finally, at $\sim$0140 UT, Cluster enters the last boundary layer near the equatorward edge of the cusp. Inside this layer, the electron temperature strongly increases, while the density is very low and close to the magnetospheric values. The trapped plasma sheet population is dominant inside this boundary layer. The magnetosheath-like population is also trapped with a well-developed loss cone. As we discussed above (section 3.4), the transition between these two boundary layers is smooth and we suggest that this boundary layer can be treated as continuation of the previous boundary layer; however, these field lines are "older," with a large part of the magnetosheath-like population having been lost in loss cone.

4.4. Comparison of Cluster and TC1 Observations

[92] There are some complications with the direct comparison of plasma populations inside the different boundary layers observed by Cluster and TC1. First, the closest conjunction in time between these satellites is when Cluster crosses into the system of equatorward boundary layers and TC1 enters the magnetosheath-like boundary layers near the dayside magnetopause. However, when Cluster is inside the cusp proper, the TC1 satellite is still inside the magnetosheath. Second, Cluster and TC1 are separated by $\sim$1.5 h MLT in the local time; thus, they are crossing different field lines. However, as suggested by previous studies, during stable northward IMF, the lobe reconnection can be stable for an extended period of time [*Fuselier et al.*, 2000b]. The spatial extent of the X-line in the lobe sector

usually covers a few hours of MLT [e.g., *Chisham et al.*, 2004; *Fear et al.*, 2005b]. The SuperDARN observations presented above agree with previous results and suggest that reconnection in the lobe sectors of both hemispheres operates at least for 1 h. The predicted footprints of the TC1 and Cluster satellites are close to each other and these two satellites can observe injections of plasma coming from the same X-line. As a result, we suggest that we can still attempt to compare plasma signatures observed by TC1 and Cluster inside the different layers. Another problem with comparison of these observations is that the interspacecraft calibrations of the plasma instruments are not yet perfect. We should also note that the magnetic field inside the cusp and inside the LLBL near dayside are different, the magnetic field magnitude at the Cluster altitude is ~150 nT, and at TC1 altitudes is ~80 nT. Thus, to perform an accurate comparison of electron populations we should perform Liouville mapping along the magnetic field. We have not yet done this, but note that if the Cluster and TC1 satellites are crossing the same field line, then Cluster would observe only part of the population seen at TC1, as some of population with near-perpendicular pitch angles will be mirrored above the Cluster satellite. Finally, comparison of the trapped high-energy electron population is problematic, as these electrons can be trapped in the region with high magnetic field and can be observed by one spacecraft but not by another. These caveats need to be noted when comparing the plasma populations inside the LLBL at the dayside and inside the midaltitude cusp.

[93] From Figure 17, one can see a very good agreement between Cluster and TC1 observations inside the low density and high temperature part of the observed populations, with $\log(N_e) < 0.8$ and $\log(T_e) > 1.8$. However, we note that Cluster detects many more points with such intermediate state than TC1. The parts of the electron population with low temperature and high density observed by both satellites do not agree that well. Of course, Cluster does not detect the PDL population and, due to the limited time interval used for the Cluster reordering, the population on newly reconnected field lines in the lobe sector of the northern hemisphere is missing in this figure. The density observed inside the cusp region is a factor of ~1.5 higher than inside the LLBL populated by the magnetosheath-like plasma. Higher densities inside the cusp, in comparison to the magnetosheath values, are often observed (B. Lavraud, private communication, 2007), which may indicate some additional trapping process inside the cusp. The most interesting result from this comparison is the identical electron densities and temperatures inside the first equatorward boundary layer near the cusp, populated by the bidirectional electrons and trapped plasma sheet population, and inside the boundary layer at dayside, which we interpreted to be on closed field lines.

[94] Comparing the electron distribution functions and plasma properties inside the different subregions of the cusp and LLBL, we suggest that we can identify some similar sublayers near the dayside magnetopause and inside the cusp. We propose that the newly open field lines outside the magnetopause observed by TC1 correspond to the poleward boundary layer inside the cusp which contains bidirectional electrons. Inside both regions, the population is bidirectional and a little heating is observed. The open field lines inside the magnetosphere observed by TC1 might correspond to the cusp proper field lines, as the electron distribution functions are very similar inside these two regions, showing a significant heating of the whole population. We have some ambiguity with the mapping of the LLBL on reclosed field lines observed by TC1, as in the Cluster observations we identify two populations on closed field line formed by dual lobe reconnection. The first population is the separate electron injections inside the cusp proper with slightly higher energy than surrounding plasma. The distribution functions inside these injections are very similar to those inside the LLBL on closed field lines near the magnetopause. The second population is the first equatorward boundary layer observed by Cluster, with a trapped plasma sheet population and a strongly bidirectional magnetosheath-like plasma. The density inside this region is similar to that observed inside the LLBL on closed field lines by TC1. However, the distribution functions are different, with electrons of magnetosheath-like energies being more bidirectional in Cluster observations in comparison to the TC1 observations. As we discussed before, this probably could be explained by the magnetic mirror effect, as only part of the electron population observed near the magnetopause will penetrate into the low altitudes. Thus, we suggest that it is more likely that the LLBL on reclosed field lines observed by TC1 maps into the first equatorward boundary layer observed by Cluster near the midaltitude cusp.

[95] The electron densities and temperatures inside the transition layer near the dayside magnetopause agree very well with those inside the second equatorward boundary layer near the cusp. Moreover, the electron distribution functions inside these regions are similar showing a loss cone and evidence of pitch angle diffusion. Thus, we suggest that the transition layer maps into the second equatorward boundary layer near the cusp. We discussed previously that inside these boundary layers a diffusion process can be important.

[96] In summary, we conclude that despite of inexact conjunction between Cluster and TC1 observations in space and time, it is possible to identify similar sublayers near the dayside magnetopause and inside the midaltitude cusp region (Figure 18). This shows that the cusp provides a snapshot of the magnetopause conditions and that reconnection is a global phenomenon as the observations can be similar even though the local time and latitude locations are different.

5. Conclusions

[97] We perform a detailed study of the structure of the LLBL observed near subsolar magnetopause by TC1 and midaltitude cusp region observed by the Cluster satellites during prolonged interval of northward IMF. We show that moving from the magnetosheath toward the dayside plasma sheet, TC1 observed a complicated structure of boundary layers: the plasma depletion layer, the magnetosheath boundary layer, populated by field lines newly reconnected in the lobe sector of the northern hemisphere, the LLBL, containing (1) open field lines, reconnected in the lobe sector of the northern hemisphere, (2) reclosed field lines, reconnected a second time in the lobe sector of the southern hemisphere, and (3) a transition layer, which is formed more likely by diffusion processes. We discuss the plasma sig-

natures inside each sublayer and show that transition parameter technique can be successfully used for the interpretation of such a complex crossing.

[98] In a similar MLT sector, Cluster, at nearly the same time moving from the lobe sector toward dayside plasma sheet, crossed the midaltitude cusp regions surrounded by boundary layers. We identify the following subregions in the Cluster data: the poleward boundary layer with reduced fluxes of the magnetosheath-like plasma, the poleward boundary layer on field lines newly reconnected in the lobe sector of the northern hemisphere, the cusp proper on open field lines which were reconnected previously, separate injections on newly reclosed field lines with higher energies than the surrounding population, the equatorward boundary layer which is formed by dual lobe reconnection, and another equatorward boundary layer which is formed more likely by diffusion processes as suggested by smooth gradients in the plasma parameters and electron pitch angle diffusion inside. Similar to TC1, we discuss plasma signatures inside each sublayer and show that we can use transition parameter technique for the reordering plasma parameters near the equatorward boundary of the cusp.

[99] Finally, we compare observations from the TC1 and LLBL satellites and suggest that the LLBL sublayers maps into the different sublayers observed in and around the cusp. Thus, the boundary layer on newly open field lines outside the magnetopause can correspond to the poleward boundary layer inside the cusp which contains bidirectional electrons (both subregions are formed by the reconnection in the lobe sector of the northern hemisphere); the open field lines inside the magnetosphere near the subsolar magnetopause correspond to the cusp proper (both are formed by the northern hemisphere lobe reconnection); the part of the LLBL with the bidirectional magnetosheath-like electron population corresponds to the first equatorward boundary near the cusp (both are formed by dual lobe reconnection processes), and the transition layer near the dayside magnetopause corresponds to the second equatorward boundary layer near the cusp. Both sublayers are formed by the diffusion processes, but they would not exist without reconnection upstream from the sublayer location.

[100] In conclusion we note that further investigation of such events is needed, which should include the study of the both electron and ion populations inside the cusp and boundary layer in order to fully understand properties of the different sublayers.

[101] **Acknowledgments.** This work is supported in the UK by the UCL/MSSL Science and Technology Facilities Council Rolling Grant. This study was born from an ISSI working group on ''Comparative Cluster-Double Star measurements of the Dayside Magnetosphere'' and the authors would like to thank ISSI, Bern, Switzerland, for its sponsorship of this group. YVB thanks B. Lavraud and I. Alexeev for fruitful discussions. We would like to thank the CDAWeb team for providing the level 2 ACE MAG and ACE Solar Wind Experiment data. We would also like to thank the PIs of the individual SuperDARN radars that have contributed the data exploited in this study.

[102] Zuyin Pu thanks the reviewers for their assistance in evaluating this paper.

References

Anderson, B. J., and S. A. Fuselier (1993), Magnetic pulsations from 0.1 to 4.0 Hz and associated plasma properties in the Earth's subsolar magnetosheath and plasma depletion layer, *J. Geophys. Res.*, *98*, 1461–1479.

Balogh, A., et al. (2001), The Cluster Magnetic Field Investigation: Overview of in-flight performance and initial results, *Ann. Geophys.*, *19*, 1207–1217.

Bauer, T. M., R. A. Treumann, and W. Baumjohann (2001), Investigation of the outer and inner low-latitude boundary layers, *Ann. Geophys.*, *19*, 1065–1088.

Bogdanova, Y. V., A. Marchaudon, C. J. Owen, M. W. Dunlop, H. U. Frey, J. A. Wild, A. N. Fazakerley, B. Klecker, J. A. Davies, and S. E. Milan (2005), On the formation of the high-altitude stagnant cusp: Cluster observations, *Geophys. Res. Lett.*, *32*, L12101, doi:10.1029/2005GL022813.

Bogdanova, Y. V., C. J. Owen, A. N. Fazakerley, B. Klecker, and H. Rème (2006), Statistical study of the location and size of the electron edge of the low-latitude boundary layer as observed by Cluster at mid-altitudes, *Ann. Geophys.*, *24*, 2645–2665.

Bogdanova, Y. V., C. J. Owen, G. Siscoe, A. N. Fazakerley, I. Dandouras, O. Marghitu, Z. Kaymaz, H. Reme, and E. A. Lucek (2007), Cluster observations of the magnetospheric low-latitude boundary layer and cusp during extreme solar wind and interplanetary magnetic field conditions: II. 07th November 2004 ICME and statistical survey, *Sol. Phys.*, *244*, 233–261, doi:10.1007/s11207-007-0418-0.

Carr, C., et al. (2005), The Double Star magnetic field investigation: instrument design, performance and highlights of the first year's observations, *Ann. Geophys.*, *23*, 2713–2732.

Chisham, G., M. Freeman, I. Coleman, M. Pinnock, M. Hairston, M. Lester, and G. Sofko (2004), Measuring the dayside reconnection rate during an interval of due northward interplanetary magnetic field, *Ann. Geophys.*, *22*, 4243–4258.

Chisham, G., et al. (2007), A decade of the Super Dual Auroral Radar Network (SuperDARN): Scientific achievements, new techniques and future directions (2007), *Surv. Geophys.*, *28*, 33–109, doi:10.1007/s10712-007-9017-8.

Cowley, S. W. H. (1973), A qualitative study of the reconnection between the Earth's magnetic field and an interplanetary field of arbitrary orientation, *Radio Sci.*, *8*, 903–913, doi:10.1029/RS008i011p00903.

Cowley, S. W. H. (1983), Interpretation of observed relationships between solar wind characteristics and effects at ionospheric altitudes, in *High Latitude Space Plasma Physics*, edited by B. Hultqvist and T. Hagfors, pp. 225–249, Plenum, New York.

Crooker, N. U. (1979), Dayside merging and cusp geometry, *J. Geophys. Res.*, *84*, 951–959, doi:10.1029/JA084iA03p00951.

Crooker, N. U. (1992), Reverse convection, *J. Geophys. Res.*, *97*, 19,363–19,372, doi:10.1029/92JA01532.

Dungey, J. W. (1961), Interplanetary magnetic field and the auroral zones, *Phys. Rev. Lett.*, *6*, 47–48, doi:10.1103/PhysRevLett.6.47.

Dungey, J. W. (1963), The structure of the ionosphere, or adventures in velocity space, in *Geophysics: The Earth's Environment*, edited by C. Dewitt, J. Hieblot, and A. Lebeau, pp. 503–550, Gordon and Breach, New York.

Eastman, T. E., and E. W. Hones Jr. (1979), Characteristics of the magnetopsheric boundary layer and magnetopause layer as observed by IMP 6, *J. Geophys. Res.*, *84*, 2019–2028, doi:10.1029/JA084iA05p02019.

Eastman, T. E., S. A. Fuselier, and J. T. Gosling (1996), Magnetopause crossings without a boundary layer, *J. Geophys. Res.*, *101*, 49–58, doi:10.1029/95JA02757.

Escoubet, C. P., M. Fehringer, and M. Goldstein (2001), Introduction: the Cluster mission, *Ann. Geophys.*, *19*, 1197–1200.

Fazakerley, A. N., et al. (2005), The Double Star Plasma Electron and Current experiment, *Ann. Geophys.*, *23*, 2733–2756.

Fear, R. C., A. N. Fazakerley, C. J. Owen, A. D. Lahiff, E. A. Lucek, A. Balogh, L. M. Kistler, C. Mouikis, and H. Rème (2005a), Cluster observations of boundary layer structure and a flux transfer event near the cusp, *Ann. Geophys.*, *23*, 2605–2620.

Fear, R. C., A. N. Fazakerley, C. J. Owen, and E. A. Lucek (2005b), A survey of flux transfer events observed by Cluster during strongly northward IMF, *Geophys. Res. Lett.*, *32*, L18105, doi:10.1029/2005GL023811.

Frey, H. U., S. B. Mende, T. J. Immel, S. A. Fuselier, E. S. Claflin, J.-C. Gérard, and B. Hubert (2002), Proton aurora in the cusp, *J. Geophys. Res.*, *107*(A7), 1091, doi:10.1029/2001JA900161.

Fujimoto, M., and T. Teresawa (1995), Anomalous ion mixing within an MHD scale Kelvin-Helmholtz vortex: 2. Effects of inhomogeneity, *J. Geophys. Res.*, *100*, 12,025–12,033, doi:10.1029/94JA02219.

Fujimoto, M., T. Mukai, H. Kawano, M. Nakamura, A. Nishida, Y. Saito, T. Yamamoto, and S. Kokubun (1998a), Structure of the low-latitude boundary layer: A case study with Geotail data, *J. Geophys. Res.*, *103*, 2297–2308, doi:10.1029/97JA02946.

Fujimoto, M., T. Teresawa, T. Mukai, Y. Saito, T. Yamamoto, and S. Kokubun (1998b), Plasma entry from the flanks of the near-Earth magnetotail: Geotail observations, *J. Geophys. Res.*, *103*, 2297–2308, doi:10.1029/97JA02946.

Fuselier, S. A., B. J. Andreson, and T. G. Onsager (1995), Particle signatures of magnetic topology at the magnetopause: AMPTE/CCE observations, *J. Geophys. Res.*, *100*, 11,805–11,821, doi:10.1029/94JA02811.

Fuselier, S. A., B. J. Anderson, and T. G. Onsager (1997), Electron and ion signatures of field line topology at the low-shear magnetopause, *J. Geophys. Res.*, *102*, 4847–4863, doi:10.1029/96JA03635.

Fuselier, S. A., K. J. Trattner, and S. M. Petrinec (2000a), Cusp observations of high- and low-latitude reconnection for northward interplanetary magnetic field, *J. Geophys. Res.*, *105*, 253–266, doi:10.1029/1999JA900422.

Fuselier, S. A., S. M. Petrinec, and K. J. Trattner (2000b), Stability of the high-Latitude reconnection site for steady northward IMF, *Geophys. Res. Lett.*, *27*, 473–476, doi:10.1029/1999GL003706.

Fuselier, S. A., S. M. Petrinec, K. J. Trattner, and W. K. Peterson (2001), O^+ observations in the cusp: Implications for dayside magnetic field topology, *J. Geophys. Res.*, *106*, 5977–5986, doi:10.1029/2000JA003030.

Gosling, J. T., M. F. Thomsen, S. J. Bame, T. G. Onsager, and C. T. Russell (1990), The electron edge of the low latitude boundary layer during accelerated flow events, *Geophys. Res. Lett.*, *17*, 1833–1836, doi:10.1029/GL017i011p01833.

Gustafsson, G., et al. (2001), First results of electric field and density observations by Cluster EFW based on initial months of operation, *Ann. Geophys.*, *19*, 1219–1240.

Haerendel, G., G. Paschmann, N. Sckopke, H. Rosenbauer, and P. C. Hedgecock (1978), The frontside boundary layer of the magnetosphere and the problem of reconnection, *J. Geophys. Res.*, *83*, 3195–3216, doi:10.1029/JA083iA07p03195.

Hall, D. S., C. P. Chaloner, D. A. Briant, D. A. Lepine, and V. P. Tritakis (1991), Electrons in the boundary layers near the dayside magnetopause, *J. Geophys. Res.*, *96*, 7869–7891, doi:10.1029/90JA02137.

Hapgood, M. A., and D. A. Bryant (1990), Re-ordered electron data in the low-latitude boundary layer, *Geophys. Res. Lett.*, *17*, 2043–2046, doi:10.1029/GL017i011p02043.

Hapgood, M. A., and D. A. Bryant (1992), Exploring the magnetospheric boundary layer, *Planet. Space Sci.*, *40*, 1431–1459, doi:10.1016/0032-0633(92)90099-A.

Hasegawa, H., M. Fujimoto, T.-D. Phan, H. Rème, A. Balogh, M. W. Dunlop, C. Hashimoto, and R. TanDokoro (2004), Transport of solar wind into Earth's magnetosphere through rolled-up Kelvin-Helmholtz vortices, *Nature*, *430*, 755–758, doi:10.1038/nature02799.

Hu, R., Y. V. Bogdanova, C. J. Owen, C. Foullon, A. N. Fazakerley, and H. Rème (2008), Cluster observations of the midaltitude cusp under strong northward IMF, *J. Geophys. Res.*, doi:10.1029/2007JA012726, in press.

Johnstone, A. D., et al. (1997), Peace: A plasma electron and current experiment, *Space Sci. Rev.*, *79*, 351–398, doi:10.1023/A:1004938001388.

Keyser, J., M. W. Dunlop, C. J. Owen, B. U. Ö. Sonnerup, S. E. Haaland, A. Vaivads, G. Paschmann, R. Lundin, and L. Rezeau (2005), Magnetopause and boundary layer, *Space Sci. Rev.*, *118*, 231–320, doi:10.1007/s11214-005-3834-1.

Lavraud, B., M. F. Thomsen, M. G. G. T. Taylor, Y. L. Wang, T. D. Phan, S. J. Schwartz, R. C. Elphic, A. Fazakerley, H. Rème, and A. Balogh (2005), Characteristics of the magnetosheath electron boundary layer under northward interplanetary magnetic field: Implications for high-latitude reconnection, *J. Geophys. Res.*, *110*, A06209, doi:10.1029/2004JA010808.

Lavraud, B., M. F. Thomsen, B. Lefebvre, S. J. Schwartz, K. Seki, T. D. Phan, Y. L. Wang, A. Fazakerley, H. Rème, and A. Balogh (2006), Evidence for newly closed magnetosheath field lines at the dayside magnetopause under northward IMF, *J. Geophys. Res.*, *111*, A05211, doi:10.1029/2005JA011266.

Le, G., C. T. Russell, J. T. Gosling, and M. F. Thomsen (1996), ISEE observations of low-latitude boundary layer for northward interplanetary magnetic field: Implications for cusp reconnection, *J. Geophys. Res.*, *101*, 27,239–27,249, doi:10.1029/96JA02528.

Liu, Z.-X., C. P. Escoubet, Z. Pu, H. Laakso, J. K. Shi, C. Shen, and M. Hapgood (2005), The Double Star mission, *Ann. Geophys.*, *23*, 2707–2712.

McComas, D. J., S. J. Bame, P. Barker, W. C. Feldman, J. L. Phillips, P. Riley, and J. W. Griffee (1998), Solar Wind Electron Proton Alpha Monitor (SWEPAM) for the Advanced Composition Explorer, *Space Sci. Rev.*, *86*, 563–612, doi:10.1023/A:1005040232597.

Milan, S. E., M. Lester, S. W. H. Cowley, and M. Brittnacher (2000), Dayside convection and auroral morphology during an interval of northward interplanetary magnetic field, *Ann. Geophys.*, *18*, 436–444, doi:10.1007/s00585-000-0436-9.

Mitchell, D. G., F. Kutchko, D. J. Williams, T. E. Eastman, L. A. Frank, and C. T. Rusell (1987), An extended study of the low-latitude boundary layer on the dawn and dusk flanks of the magnetopause, *J. Geophys. Res.*, *92*, 7394–7404, doi:10.1029/JA092iA07p07394.

Newell, P. T., and C.-I. Meng (1988), The cusp and the cleft/boundary layer- Low-altitude identification and statistical local time variation, *J. Geophys. Res.*, *93*, 14,549–14,556, doi:10.1029/JA093iA12p14549.

Newell, P. T., and C.-I. Meng (1992), Mapping the dayside ionosphere to the magnetosphere according to particle precipitation characteristics, *Geophys. Res. Lett.*, *19*, 609–612, doi:10.1029/92GL00404.

Nykyri, K., A. Otto, B. Lavraud, C. Mouikis, L. M. Kistler, A. Balogh, and H. Rème (2006), Cluster observations of reconnection due to the Kelvin-Helmholtz instability at the dawnside magnetospheric flank, *Ann. Geophys.*, *24*, 2619–2643.

Ogilvie, K. W., and G. J. Fitzenreiter (1989), The Kelvin-Helmholtz instability at the magnetopause and inner boundary layer surface, *J. Geophys. Res.*, *94*, 15,113–15,123, doi:10.1029/JA094iA11p15113.

Ogilvie, K. W., R. J. Fitzenreiter, and J. D. Scudder (1984), Observations of electron beams in the low-latitude boundary layer, *J. Geophys. Res.*, *89*, 10,723–10,732, doi:10.1029/JA089iA12p10723.

Øieroset, M., J. Raeder, T. D. Phan, S. Wing, J. P. McFadden, W. Li, M. Fujimoto, H. Rème, and A. Balogh (2005), Global cooling and densification of the plasma sheet during an extended period of purely northward IMF on October 22–24, *Geophys. Res. Lett.*, *32*, L12S07, doi:10.1029/2004GL021523.

Onsager, T. G., and J. D. Scudder (2002), Low-latitude boundary layer formation by magnetic reconnection, in *Earth's Low-Latitude Boundary Layer*, *Geophys. Monogr. Ser.*, vol. 133, edited by P. T. Newell and T. Onsager, pp. 111–120, AGU, Washington, D. C.

Onsager, T. G., J. D. Scudder, M. Lockwood, and C. T. Russell (2001), Reconnection at the high-latitude magnetopause during northward interplanetary magnetic field conditions, *J. Geophys. Res.*, *106*, 25,467–25,488, doi:10.1029/2000JA000444.

Paschmann, G. (1979), Plasma structure of the magnetopause and boundary layer, in *Magnetopsheric Boundary Layers*, edited by J. Lemaire, *Eur. Space Agency Spec. Publ., ESA SP*, *148*, 25.

Paschmann, G., W. Baumjohann, N. Sckopke, T.-D. Phan, and H. Luhr (1993), Structure of the dayside magnetopause for low magnetic shear, *J. Geophys. Res.*, *98*, 13,409–13,422, doi:10.1029/93JA00646.

Petrinec, S. M., and C. T. Russell (1995), An examination of the effect of dipole tilt angle and cusp regions on the shape of the dayside magnetopause, *J. Geophys. Res.*, *100*, 9559–9566, doi:10.1029/94JA03315.

Phan, T. D., et al. (1997), Low-latitude dusk flank magnetosheath, magnetopause, and boundary layer for low magnetic shear: Wind observations, *J. Geophys. Res.*, *102*, 19,883–19,896, doi:10.1029/97JA01596.

Phan, T.-D., M. Oieroset, and M. Fujimoto (2005), Reconnection at the dayside low-latitude magnetopause and its nonrole in low-latitude boundary layer formation during northward interplanetary magnetic field, *Geophys. Res. Lett.*, *32*, L17101, doi:10.1029/2005GL023355.

Provan, G., M. Lester, S. W. H. Cowley, A. Grocott, S. E. Milan, B. Hubert, and H. Khan (2005), Modulation of dayside reconnection during northward interplanetary magnetic field, *J. Geophys. Res.*, *110*, A10211, doi:10.1029/2004JA010980.

Reiff, P. H., T. W. Hill, and J. L. Burch (1977), Solar wind plasma injection at the dayside magnetopause, *J. Geophys. Res.*, *82*, 479–491, doi:10.1029/JA082i004p00479.

Rème, H., et al. (2001), First multispacecraft ion measurements in and near the Earth's magnetosphere with the identical Cluster ion spectrometry (CIS) experiment, *Ann. Geophys.*, *19*, 1303–1354.

Rème, H., et al. (2005), The HIA instrument on board the Tan Ce 1 Double Star near-equatorial spacecraft and its first results, *Ann. Geophys.*, *23*, 2757–2774.

Ruohoniemi, J. M., and K. B. Baker (1998), Large-scale imaging of high latitude convection with Super Dual Auroral Radar Network HF radar observations, *J. Geophys. Res.*, *103*, 20,797–20,811, doi:10.1029/98JA01288.

Sandholt, P. E., C. J. Farrugia, S. W. H. Cowley, M. Lester, W. F. Denig, J.-C. Cerisier, S. E. Milan, J. Moen, E. Trondsen, and B. Lybekk (2000), Dynamic cusp aurora and associated pulsed reverse convection during northward interplanetary magnetic field, *J. Geophys. Res.*, *105*, 12,869–12,894, doi:10.1029/2000JA900025.

Shapiro, V. D., V. I. Shevchenko, P. J. Cargill, and K. Papadopoulos (1994), Modulational instability of lower hybrid waves at the magnetopause, *J. Geophys. Res.*, *99*, 23,735–23,470, doi:10.1029/94JA02074.

Smith, C. W., J. L'Heureux, N. F. Ness, M. H. Acuña, L. F. Burlaga, and J. Scheifele (1998), The ACE Magnetic Fields Experiment, *Space Sci. Rev.*, *86*, 613–632, doi:10.1023/A:1005092216668.

Smith, M. F., and M. Lockwood (1996), Earth's magnetospheric cusps, *Rev. Geophys.*, *34*, 233–260, doi:10.1029/96RG00893.

Song, P., and C. T. Russell (1992), Model of the formation of the low-latitude boundary layer for strongly northward interplanetary magnetic field, *J. Geophys. Res.*, *97*, 1411–1420, doi:10.1029/91JA02377.

Song, P., R. C. Elphic, C. T. Russell, J. T. Gosling, and C. A. Cattell (1990), Structure and properties of the subsolar magnetopause for northward IMF: ISSE observations, *J. Geophys. Res.*, *95*, 6375–6387, doi:10.1029/JA095iA05p06375.

Song, P., C. T. Russell, R. J. Fitzenreiter, J. T. Gosling, M. F. Thomsen, D. G. Mitchell, S. A. Fuselier, G. K. Parks, R. R. Anderson, and D. Hubert (1993), Structure and properties of the subsolar magnetopause for northward interplanetary magnetic field: Multiple-instrument particle observations, *J. Geophys. Res.*, *98*, 11,319–11,337, doi:10.1029/93JA00606.

Song, P., C. T. Russell, T. I. Gombosi, and D. L. DeZeeuw (2002), A model of the formation of the low-latitude boundary layer for northward IMF by reconnection: A summary and review, in *Earth's Low-Latitude Boundary Layer*, *Geophys. Monogr. Ser.*, vol. 133, edited by P. T. Newell and T. Onsager, pp. 121–130, AGU, Washington, D. C.

Stubbs, T. J., P. J. Cargill, M. Lockwood, M. Grande, B. J. Kellett, and C. H. Perry (2004), Extended cusp-like regions and their dependence on the Polar orbit, seasonal variations, and interplanetary conditions, *J. Geophys. Res.*, *109*, A09210, doi:10.1029/2003JA010163.

Treumann, R. A., and W. Baumjohann (1988), Particle trapping at a tangential discontinuity: Multiple incidence, *Planet. Space Sci.*, *36*, 1477–1491, doi:10.1016/0032-0633(88)90013-X.

Treumann, R. A., J. LaBelle, and T. M. Bauer (1995), Diffusion processes: An observational perspective, in *Physics of the Magnetopause*, *Geophys. Monogr. Ser.*, vol. 90, edited by P. Song, B. U. Ö. Sonnerup, and M. F. Thomsen, pp. 331–340, AGU, Washington, D. C.

Tsyganenko, N. A. (1995), Modeling the Earth's magnetospheric magnetic field confined within a realistic magnetopause, *J. Geophys. Res.*, *100*, 5599–5612, doi:10.1029/94JA03193.

Twitty, C., T. D. Phan, G. Paschmann, B. Lavraud, H. Rème, and M. Dunlop (2004), Cluster survey of cusp reconnection and its IMF dependence, *Geophys. Res. Lett.*, *31*, L19808, doi:10.1029/2004GL020646.

Vaisberg, O. L., V. N. Smirnov, L. A. Avanov, J. H. Waite, J. L. Burch, D. L. Gallagher, and N. L. Borodkova (2001), Different types of low-latitude boundary layer as observed by Interball Tail probe, *J. Geophys. Res.*, *106*, 13,067–13,090, doi:10.1029/2000JA000154.

Watanabe, M., G. J. Sofko, D. A. Andre, J. M. Ruohoniemi, M. R. Hairston, and K. Kabin (2006), Ionospheric signatures of internal reconnection for northward interplanetary magnetic field: Observation of 'reciprocal cells' and magnetosheath ion precipitation, *J. Geophys. Res.*, *111*, A06201, doi:10.1029/2005JA011446.

Y. V. Bogdanova, Department of Physics, La Trobe University, Melbourne, Vic 3086, Australia. (jb@mssl.ucl.ac.uk)

C. M. Carr and E. A. Lucek, Space and Atmospheric Physics, Blackett Laboratory, Imperial College London, Prince Consort Road, London SW7 2BW, UK.

I. Dandouras and H. Rème, Centre d'Etude Spatiale des Rayonnements, Centre National de la Recherche Scientifique, 9 Avenue du Colonel Roche, F-31028 Toulouse, France.

J. A. Davies and M. W. Dunlop, Space Science and Technology Department, Rutherford Appleton Laboratory, Didcot OX11 0QX, UK.

A. N. Fazakerley, A. D. Lahiff, and C. J. Owen, Mullard Space Science Laboratory, University College London, Holmbury St. Mary, Dorking RH5 6NT, UK.

M. G. G. T. Taylor, Research and Scientific Support Department, European Space Agency, Keplerlaan 1, NL-2201 AZ Noordwijk ZH, Netherlands.

J. A. Wild, Department of Communication Systems, Lancaster University, Lancaster LA1 4WA, UK.